3D J-integral evaluation for solids undergoing large elastic plastic deformations with residual stresses and spatially varying mechanical properties of a material

doi: 10.1016/j.engfracmech.2020.107212

3D J-integral evaluation for solids undergoing large elastic-plastic deformations with residual stresses and spatially varying mechanical properties of a material

Hiroshi Okada[1]*, Tatsuro Ishizaka[2], Akira Takahashi[3], Koichiro Arai[4] and Yasunori Yusa[5]

1*) Corresponding author, Professor, Department of Mechanical Engineering, Faculty of Science and Technology
Tokyo University of Science, 2641 Yamazaki, Noda 278-5810, Japan,
hiroshi.okada@rs.tus.ac.jp
2) Graduate Student, Department of Mechanical Engineering, Faculty of Science and Technology, Tokyo University of Science (Currently, MSC Software Corporation, Japan), tatsuro.ishizaka@hexagon.com
3) Graduate Student, Department of Mechanical Engineering, Faculty of Science and Technology, Tokyo University of Science (Currently, Nippon Steel Corporation, Japan), takahashi.aq6.akira@jp.nipponsteel.com
4) Graduate Student, Department of Mechanical Engineering, Faculty of Science and Technology, Tokyo University of Science (Currently, MSC Software Corporation, Japan), koichiro.arai@hexagon.com
5) Department of Mechanical and Intelligent Systems Engineering, Graduate School of Informatics and Engineering, The University of Electro-Communications, 1-5-1 Chofugaoka, Chofu, Tokyo 182-8585, Japan, y.yusa@uec.ac.jp

Abstract

In this paper, a 3D J-integral based on the domain integral approach is presented for large deformation elastic-plastic fracture mechanics problems associated with residual stresses and spatially varying mechanical properties of a material. The proposed 3D J-integral has physical significance as the energy dissipation into the process zone. The derivations of the proposed J-integral are presented in detail. Through numerical examples, it is shown that the proposed J-integral is unconditionally path independent. The present formulation is a rigorous extension of the 2D-T_ε^* integral of Okada and Atluri to 3D.

Highlights

- The proposed 3D J-integral is unconditionally path-independent (PI).
- The PI property holds in large deformation elastic-plastic problems.
- The PI property is guaranteed for problems with residual stresses.
- The PI property is valid for problems with spatially varying mechanical properties.
- The PI properties are demonstrated in example problems.

Keywords

J-integral; Energy release rate; Domain integral method; Elastic-plastic fracture; Functionally graded material (FGM)

Nomenclature

B^o: Original undeformed configuration

V^o: Volume of the original undeformed configuration

$\boldsymbol{X}^o \left(X_1^o, X_2^o, X_3^o \right)$: Position of a material point in the original undeformed configuration

B^{Prior}: Configuration after prior deformation

V^{Prior}: Volume of the configuration after prior deformation

$\boldsymbol{X}^{\text{Prior}} \left(X_1^{\text{Prior}}, X_2^{\text{Prior}}, X_3^{\text{Prior}} \right)$: Position of a material point in the configuration after prior deformation

u_i^{Prior}: Displacements of a material point, from the original undeformed configuration to that after prior deformation

F_{ij}^{Prior}: Deformation gradients at a material point, from the original undeformed configuration to that after prior deformation

u_i^{Mech}: Displacements of a point due to generation of a crack and applied loads

$\Delta F_{ij}^{\text{Mech}}$: Increments of the displacement gradients at a point due to generation of a crack and applied loads

π_{ij}: Nominal stresses at a point (reference configuration is B^o)

Q_{ijkl}: Fourth-order tensor expressing the increments of nominal stresses π_{ij} with respect to those of deformation gradients F_{kl}

π_{ij}^{Prior} : Nominal stresses at a point after prior deformation (reference configuration is B^o)

W^o: Strain energy density referring to B^o

W^{Prior} and W^{Mech} : Strain energy densities due to prior deformation and due to generation of a crack and applied loads

$U^{Int.}$: Internal energy

$U^{Ext.}$: External work

$\bar{t}_i^o$ and G_i^o: Prescribed tractions and body forces per unit volume

a and Δa: Crack length and its small increment

G: Energy release rate

$\frac{D}{Da}$: Differential operator with respect to crack length a.

∂V_t^o: Traction prescribed boundary of volume V^o

V_ε^o and ∂V_ε^o: Small volume (region) surrounding the crack tip and its outer boundary (2D), or inside a small cylinder of radius and length e and its cylindrical surface (3D)

ε: Radius of V_ε^o

N_i^ε: Unit outward normal vector on ∂V_ε^o

t_i^o: Tractions on ∂V_ε^o

$\hat{G}$: Energy dissipation into a process zone of radius ε and width unity, per unit crack extension

$q\left(\boldsymbol{X}^o\right)$: A function of $\boldsymbol{X}^o$ which is continuous and piece-wise differentiable in the integral domain. It also expresses the virtual crack extension when $\boldsymbol{X}^o$ is at the crack front.

$V_{Int.}^o$: Region surrounding the crack tip

δ: Virtual crack extension at the crack tip

$\partial V_{\varepsilon-\mathrm{end}(+)}^o$ and $\partial V_{\varepsilon-\mathrm{end}(-)}^o$: End surfaces of V_ε^o for the 3D problem

b^o: Length of V_ε^o in the 3D problem

A_ε^o and ∂A_ε^o: Small disk obtained by degenerating V_ε^o and its periphery

Ω_ε^o and Δ: Small volume assumed for the proposed domain integral method and its length along the crack front

$\partial\Omega_{Int}^o$: Volume of integral domain

r^o: Radius of the assumed integral domain

w^o: Width of the assumed integral domain at the outer radius

E and σ_Y: Young's modulus and yield stress

1. Introduction

In this paper, the computations of the three-dimensional J-integral for solids with residual stresses and with spatially varying mechanical properties of material are discussed. They are induced by deformation histories before the onsets of cracks. We call any deformations before the onsets of cracks prior deformations, in this article. Engineering structures are often subject to elastic-plastic or thermo-elastic-plastic deformations during their manufacturing processes. For example, the processes in welding generally involve very complex thermo-elastic-plastic deformations, as described in earlier literature on welding mechanics (Ueda et al. [1, 2]). As a result, residual stresses develop in the welded joints as well as in the vicinity of the welded joints. Research on the prediction of weld residual stress has been presented in previous studies (for example, Maekawa et al. [3,4] and Broussard [5]). The weld analyses are known to be very complex and difficult as they involve very complicated thermo-mechanical nonlinear analyses. Variabilities in analysis results have been an issue. Plastic works such as the cold expansion of a hole are known to generate compressive surface residual stress, enhancing the fatigue lives of structures (for example, Chakherlou and Vogwell [6], Pavier et al [7], and Marannano [8]). Other metal forming processes, such as drawing and stamping, are known to produce residual stresses as the finite element analyses were presented by Rasty and Chapman [9] and Yang et al. [10]. Hence, the influences of residual stresses in the structure need to be taken into consideration for the fracture parameter evaluations of real engineering structures, as presented by Nose et al. [11] as an example. In Nose et al. [11], the stress intensity factors were computed by the virtual crack closure-integral method (VCCM) proposed by Okada et al. [12] with the consideration of distributed weld residual stresses.

The complex thermo-elastic-plastic deformation sometimes influences the mechanical properties of a material, such as yield stress. Metal forming processes are associated with plastic deformations, developing residual stresses. Numerous publications can be found in the literature. They include the measurements of spatially varying stress-strain relationships in the weld metal and the heat affected zone of the welded joint, as presented by Yonezu et al. [13] and Kim et al. [14]. In the case of functionally graded materials (FGMs), the mechanical properties of the material vary in a controlled manner. Functionally graded materials were proposed by researchers in the field of aerospace engineering to reduce thermal stress when the structure was subjected to a severe thermal environment. The early development of FGM is summarized in the review articles of Niino et al. [15] and Koizumi [16]. The production method of FGMs seems to be evolving

in recent years. We can find the centrifugal method to manufacture FGM pipes as described in the review article of Watanabe et al. [17]. More recently, the additive manufacturing technique was applied to produce FGM, as seen in the article of Zuback et al. [18]. One can assume that, due to the thermo-elastic-plastic deformation during the fabrication process, residual stresses develop in the structure, in addition to the spatially varying mechanical properties due to the material composition gradients.

On the other hand, metallic structures generally deform largely in the event of structural failure. We can find a series of research reports of Hojo et al. [19, 20, 21]. The articles of Hojo et al. reported the ductile crack growth behaviors of compact tension specimens under large amplitudes of cyclic loads and their finite element analyses. The experimental specimens deformed largely. Other examples of fracture behaviors of metallic structures can be seen in the Sandia fracture challenge, as summarized in Boyce et al. [22, 23] and Kramer et al. [24]. Blind round-robin analyses were carried out. It has had three phases up to the present day. Here, 13, 14 and 21 teams participated in the first, second, and third phases, respectively. The first and second phases dealt with a martensitic stainless steel and titanium alloy specimens undergoing very complex fracture behaviors. The third phase was carried out on additive manufactured experimental specimens made of a stainless steel powder. In all cases, cracks propagated in complex manners as they were subject to mixed-mode conditions. Most importantly, the specimens were found to experience large deformations before complete fracture occurred.

Thus, we defined our challenge in the present research as follows. As stated above, metallic structures often have residual stresses and spatially varying mechanical properties of the material. Furthermore, the structures often undergo large deformations before fracture. The objective of the present research is to develop a methodology to evaluate fracture mechanics parameter that is applicable to all of the aforementioned scenarios in a unified fashion.

The J-integral (Rice [25]) was proposed as the energy release rate associated with the extension of a two-dimensional crack. A homogeneous elastic material was assumed in the derivation of the two-dimensional J-integral. The J-integral has the same integral formulation as the Energy Momentum Tensor of Eshelby [26] which was the general force on defect in solid. Cherepanov [27] also presented a contour integral formulation that expressed the energy release rete. The contour integral of Cherepanov [27] was essentially the same as the J-integral. The J-integral could be evaluated on an arbitrary integral

contour surrounding the crack tip. This is known as the “path-independent property” of the J-integral. It is the key feature of the J-integral. Although the J-integral of Rice [27] assumed a homogeneous material, one can show that the material needs to be homogenous only in the direction of crack. The two-dimensional J-integral was extended to the three-dimensional formulation by Blackburn [28]. In Blackburn [28], the three-dimensional J-integral was represented by the contour integral accompanied by an integral over an area inside the integral contour. Amestoy et al. [29] gave further insights to the formulation for a nonlinear material case. Kubo, et al. [30] proposed the global J scalar which was based on a very similar concept as that of the domain integral approach. Kikuchi et al. [31, 32] and Ando et al. [3] presented the numerical evaluations of the J-integral from the results of the three-dimensional finite element analysis. Kikuchi et al. [31] analyzed problems of semi-elliptical surface flaw developed at the inner wall of a pressure vessel. Then, they presented elastic-plastic analysis of CT specimen in their following article [32]. Ando et. al. [33] dealt with thermal-elastic-plastic facture problems. The domain integral method was proposed along with the concept of virtual crack extension (see, for example, Li et al. [34] and de Lorenzi [35]). The domain integral approach is especially suited to the finite element method, as the quadrature rules embedded in the finite element program can carry out the volume integral, as presented by Nikishkov and Atluri [36, 37]. The J-integral value is independent of the shape and size of the integral domain. Such a property is also called the path-independent property. The path independent property, in a rigorous sense, can be guaranteed for elastic materials only, whose elastic constants do not change in the direction of crack.

For two-dimensional general nonlinear materials undergoing arbitrary deformation histories, the T^* integral was proposed by Atluri, Nishioka and Nakagaki [38]. In Atluri, Nishioka, and Nakagaki [38], an integral formulation on an infinitesimally small contour surrounding the crack tip was formulated based on an arbitrary incremental constitutive law. It expressed the energy flowing into an infinitesimally small area surrounded by the integral path. The integral was converted to an integral on an arbitrary contour path associated with an area integral for which the integral domain is inside the contour. The T^* integral was applied to various nonlinear fracture mechanics problems including elastic-plastic stable crack propagation and thermal fracture problem (Brust et al. [39, 40]). Okada and Atluri [41] reformulated the T^* integral as an integral on a small but

finite contour path surrounding the crack tip. Two kinds of small integral contours were proposed. One was the moving contour path. The other was the elongating contour path. The moving path moves with the location of crack tip as the crack extends. The elongating path extends its length as the crack propagates. Okada and Atluri [41] showed that the moving path expressed the energy release rate at the crack tip. The elongating path was the energy dissipated into the area surrounding the contour per unit crack growth. The size ε of the integral contours was found to influence the value of the T^*. They renamed this integral as the T_ε^* integral. It was applied to characterize stable crack propagations in metallic plates (Omori, et al. [42] and Okada, et al. [43]).

The J-integral was applied to the finite strain problems by Carka and Landis [44] and Carka et al. [45]. They found that the J-integral lost its path-independent property in finite deformation problems. Koshima and Okada [46] presented a three-dimensional J-integral based on the domain integral method. To retain the path-independent property, the second integral, which contained the spatial derivatives of the strain energy density and the displacement gradients in its integrand, was introduced. The second integral recovered the path-independent property. A numerical scheme based on the superconvergent patch recovery method of Zienkiewicz and Zhu [47, 48] was introduced for the computation of the spatial derivatives. Recently, Arai, Okada, and Yusa [49, 50] proposed a three-dimensional J-integral formulation that was path independent even for elastic-plastic solids undergoing large cyclic deformations. It was a rigorous extension of the two-dimensional T_ε^* integral to the three-dimensional problem using the domain integral method along with the virtual crack extension. Arai, Okada, and Yusa [51] extended the three-dimensional J-integral to the computation of ΔJ for fatigue problems involving significant plastic deformations.

For linear fracture mechanics problems, Yildirim [52] presented the J-integral approach for FGMs under thermal stresses. Moghaddam and Alfano [53] presented analyses of the 3D-curved cracks in FGMs subject to thermal loading. Hein and Kuna [54] dealt with materials having temperature-dependent mechanical properties. Park et al. [55] presented a two-dimensional formulation in the presence of residual and thermal stresses. Jin and Dodds Jr. [56] extended the 3D J-integral formulation to the case of elastic-plastic problems in which the explicit derivatives of the strain energy density can be computed

by simple formulae. Wang and Nakamura [57] presented elastic-plastic problems of FGMs. Recently, Okada et al. [58] proposed a J-integral computation methodology based on the domain integral approach that can allow the spatial variations in mechanical properties of materials, including Young's modulus, yield stress, and the stress-strain relationship. All studies listed in this paragraph are limited in infinitesimally small strain problems, and large-strain elastic-plastic problems were not considered.

In the present investigation, appropriate ways to include the influences of the residual stresses and of spatially varying mechanical properties of material in the evaluation of the three-dimensional J-integral applicable to large deformation elastic-plastic fracture mechanics analysis have been sought. The domain integral method was adopted for its evaluation. Although the residual stresses are induced during the prior deformations, we assumed that the complete deformation histories were not known. However, the residual stresses and the shape of structure after the prior deformations were assumed to be known. The residual stresses may be measured by an experimental technique. Then, due to the applied load, the structure was assumed to undergo a large deformation for which the finite strain formulation based on the total Lagrange description was adopted in the J-integral formulation. Under the assumptions on the prior-deformation histories, a three-dimensional J-integral formulation having the path-independent property is proposed in this paper. The formulation of the proposed three-dimensional J-integral is derived in Section 2. Some numerical examples demonstrating the capabilities of the proposed J-integral formulation are given in Section 3. Finally, some discussions and conclusions are given in Sections 4 and 5. The proposed J-integral formulation expresses energy dissipating into a small piped region surrounding a crack front of length unity per unit crack extension.

2. Three-dimensional J-integral formulation for solids with residual stresses and spatially varying mechanical properties of a material undergoing large deformation

In this section, some discussions on the notations of prior deformation histories are given first, followed by those on the two-dimensional J-integral formulation. Then, it is extended to the three-dimensional case. The two-dimensional J-integral is defined on a small integral contour Γ_ε surrounding the crack tip. Then, the three-dimensional formulation based on the virtual crack extension and the domain integral method is

derived following Arai et al. [49, 50]. It is noted that the material is not assumed to be homogeneous in the processes of deriving the domain integral method. Therefore, the present J-integral formulation can be applied to problems with spatially varying mechanical properties of a material, such as Young's modulus and yield stress.

2.1 Notions of deformation: deformation gradients and displacement gradients

Figure 1 schematically presents the deformations of the body from its original undeformed configuration to the final deformed state. In the original undeformed configuration B^o, the body is assumed to be free from any strains and stresses. The volume and the coordinates of a material point in the configuration B^o are denoted by V^o and $\boldsymbol{X}^o\left(X_1^o, X_2^o, X_3^o\right)$, respectively. In this configuration, the body does not have any cracks. We denote the configuration after the prior deformations by B^{Prior}. The body and the position of a material point are denoted by V^{Prior} and $\boldsymbol{X}^{\text{Prior}}$ $\left(X_1^{\text{Prior}}, X_2^{\text{Prior}}, X_3^{\text{Prior}}\right)$, respectively. Also, cracks do not exist in this configuration. The displacements of a point from B^o to B^{Prior} are expressed by u_i^{Prior}. Thus, the deformation gradients due to the prior deformation are expressed as follows:

$$F_{ij}^{\text{Prior}} = \delta_{ij} + \frac{\partial u_i^{\text{Prior}}}{\partial X_j^o} \cdots\cdots (1)$$

Then, the deformations due to the generation of the crack and the mechanical loads follow. The body reaches the deformed configuration B, the volume of which is denoted by V. The displacements of a point from the configurations B^{Prior} to B are expressed by u_i^{Mech}. Hence, the deformation gradients F_{ij} can be expressed as follows:

$$F_{ij} = \frac{\partial x_i}{\partial X_j^o} = \delta_{ij} + \frac{\partial u_i}{\partial X_j^o} = \delta_{ij} + \frac{\partial u_i^{\text{Prior}}}{\partial X_j^o} + \frac{\partial u_i^{\text{Mech}}}{\partial X_j^o} = F_{ij}^{\text{Prior}} + \Delta F_{ij}^{\text{Mech}} \cdots\cdots (2)$$

where $\Delta F_{ij}^{\text{Mech}} = \dfrac{\partial u_i^{\text{Mech}}}{\partial X_j^o}$ are the increments in the displacement gradients due to the

creation of the crack and the applied loads.

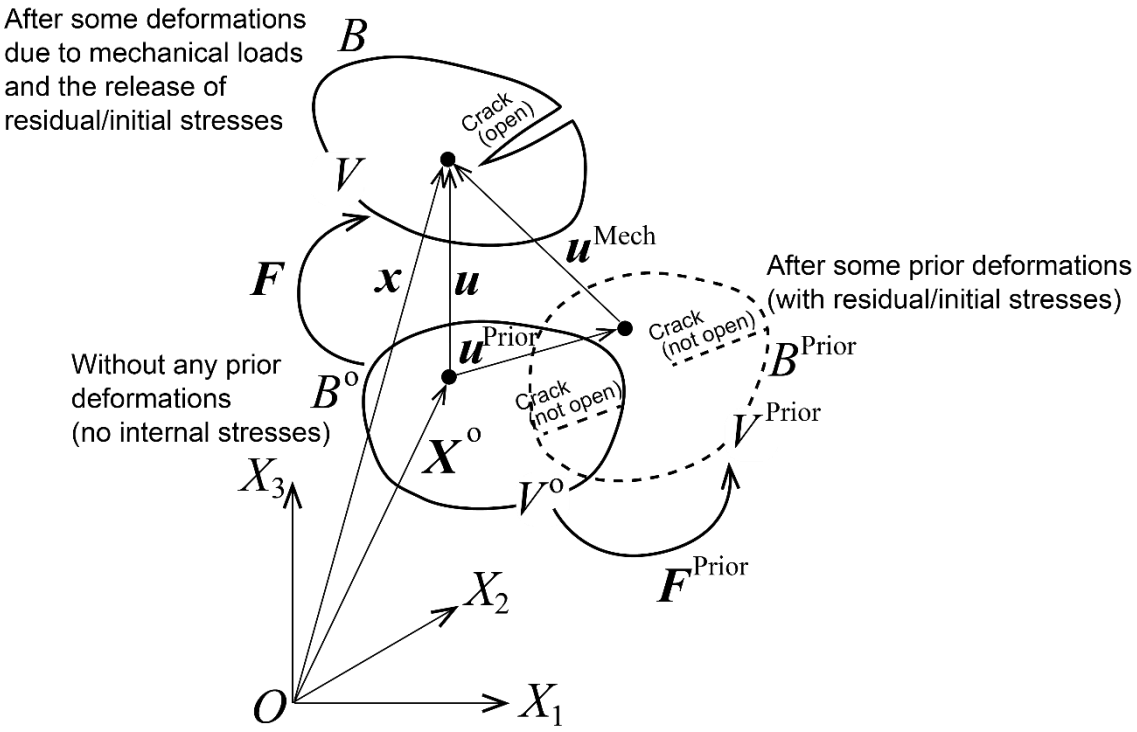

Figure 1 Notions of the prior deformation and that due to the mechanical loads and the release of residual/initial stresses.

2.2 Stresses and strain energy

The nominal stresses having the reference configuration B^o are denoted by π_{ij}. The nominal stresses can be expressed by their evolution equation:

$$\pi_{ij} = \int_0^{F_{kl}} Q_{ijkl}\left(\hat{F}_{mn}\right) \mathrm{d}\hat{F}_{kl} \cdots\cdots (3)$$

Here, equation (3) is a generic form to express the stress evolution. Moreover, Q_{ijkl} are the components of fourth-order tensor expressing the increments of nominal stresses π_{ij} with respect to those of deformation gradients F_{kl}. While the mechanical loads are being applied to the body, we may write

$$\pi_{ij} = \pi_{ij}^{\mathrm{Prior}} + \int_0^{\Delta F_{kl}^{\mathrm{Mech}}} Q_{ijkl}\left(\Delta \hat{F}_{mn}^{\mathrm{Mech}}\right) \mathrm{d}\left(\Delta \hat{F}_{kl}^{\mathrm{Mech}}\right). \quad \cdots\cdots (4)$$

The strain energy density W^o per unit volume of the configuration V^o can be written in its generic from as

$$W^o = \int_0^{F_{ij}} \pi_{ij}\left(\hat{F}_{mn}\right) \mathrm{d}\hat{F}_{ji}. \quad \cdots\cdots (5)$$

The strain energy density while the mechanical loads are being applied can be expressed by an alternative form as

$$W^o = W^{\mathrm{Prior}} + W^{\mathrm{Mech}}. \quad \cdots\cdots (6)$$

Here, W^{Prior} and W^{Mech} are the strain energy densities due to the prior deformation and due to the creation of the crack and the applied loads, respectively. They are expressed as

$$\begin{aligned} W^{\mathrm{Prior}} &= \int_0^{F_{ji}^{\mathrm{Prior}}} \pi_{ij}\left(\hat{F}_{mn}^{\mathrm{Prior}}\right) \mathrm{d}\hat{F}_{ji}^{\mathrm{Prior}} \\ W^{\mathrm{Mech}} &= \int_0^{\Delta F_{ji}^{\mathrm{Mech}}} \pi_{ij}\left(\Delta \hat{F}_{mn}^{\mathrm{Mech}}\right) \mathrm{d}\Delta \hat{F}_{ji}^{\mathrm{Mech}} \end{aligned}. \quad \cdots\cdots (7)$$

The strain energy density due to the prior deformation and to the mechanical loads can be decomposed, as shown in equation (7).

2.3 Expressions for the energy release rate in the two-dimensional problem

As a preliminary discussion, we first consider the two-dimensional crack propagation problem under the boundary conditions, as depicted in Figure 2 (a). The internal energy $U^{Int.}$ can be written as follows:

$$U^{Int.} = \int_{V^o} W^o \mathrm{d}V^o \quad \cdots\cdots (8)$$

External work $U^{Ext.}$ due to the prescribed tractions $\bar{t}_i^o$ and the body forces per unit volume G_i^o acting in the body can be written as

$$U^{Ext.} = \int_{\partial V_t^o} \bar{t}_i^o u_i \mathrm{d}\left(\partial V_t^o\right) + \int_{V^o} G_i^o u_i \mathrm{d}\left(V^o\right). \quad \cdots\cdots (9)$$

Following the discussions of Atluri, Nishioka, and Nakagaki [38], we discuss the change of energies while the crack extends for a small length Δa in the X_1^0 direction. The energy G released at the crack tip can be written as

$$G\Delta a = \frac{DU^{Ext.}}{Da}\Delta a - \frac{DU^{Int.}}{Da}\Delta a\,. \quad \cdots\cdots (10)$$

Here, $\frac{D}{Da}$ is the differential operator with respect to the crack length a. Using equations (8) and (9), we can rewrite the expression (10) as

$$G = \int_{\partial V_t^o} \bar{t}_i^o \frac{Du_i}{Da} \mathrm{d}\left(\partial V_t^o\right) + \int_{V^o} G_i^o \frac{Du_i}{Da} \mathrm{d}V^o - \frac{D}{Da}\int_{V^o} W \mathrm{d}V^o\,. \quad \cdots\cdots (11)$$

As shown in Figure 2 (a), we introduce the region V_ε^o in the immediate vicinity of the crack tip. Hence, equation (11) can be shown in an alternative expression as

$$\begin{aligned} G = {} & \int_{\partial V_t^o} \bar{t}_i^o \frac{Du_i}{Da} \mathrm{d}\left(\partial V_t^o\right) - \int_{\partial V_\varepsilon^o} t_i^o \frac{Du_i}{Da} \mathrm{d}\left(\partial V_\varepsilon^o\right) + \int_{V^o - V_\varepsilon^o} G_i^o \frac{Du_i}{Da} \mathrm{d}\left(V^o - V_\varepsilon^o\right) \\ & - \int_{V^o - V_\varepsilon^o} \pi_{ij} \frac{DF_{ji}}{Da} \mathrm{d}\left(V^o - V_\varepsilon^o\right) \\ & + \int_{\partial V_\varepsilon^o} t_i^o \frac{Du_i}{Da} \mathrm{d}\left(\partial V_\varepsilon^o\right) + \int_{V_\varepsilon^o} G_i^o \frac{Du_i}{Da} \mathrm{d}\left(V_\varepsilon^o\right) - \frac{D}{Da}\int_{V_\varepsilon^o} W \mathrm{d}V_\varepsilon^o \end{aligned} \quad . (12)$$

In equation (12), the nominal stresses π_{ij} are expressed using the relationships $\pi_{ij} = \partial W / \partial F_{ji}$ that can be obtained from equation (8). Moreover, ∂V_ε^o is the outer boundary of region V_ε^o, as depicted in Figure 2(b). The tractions t_i^o on ∂V_ε^o are expressed by the unit outward normal vector N_i^ε and the nominal stresses π_{ij} as

$$t_i^o = N_j^\varepsilon \pi_{ji}\,. \quad \cdots\cdots (13)$$

When the body is in equilibrium, the following relationship holds:

$$0=\int_{\partial V_t^o}\bar{t}_i^o\frac{Du_i}{Da}\mathrm{d}\left(\partial V_t^o\right)-\int_{\partial V_\varepsilon^o}t_i^o\frac{Du_i}{Da}\mathrm{d}\left(\partial V_\varepsilon^o\right)$$
$$+\int_{V^o-V_\varepsilon^o}G_i^o\frac{Du_i}{Da}\mathrm{d}\left(V^o-V_\varepsilon^o\right)-\int_{V^o-V_\varepsilon^o}\pi_{ij}\frac{DF_{ji}}{Da}\mathrm{d}\left(V^o-V_\varepsilon^o\right) \quad \cdots\cdots\cdots\cdots\cdots (14)$$

This equation expresses the virtual work principle for the body $V^o-V_\varepsilon^o$ when $\frac{Du_i}{Da}$ are considered as the variations of the displacements. Hence, by letting the radius ε of the volume V_ε^o to be zero in the limit, the energy release rate at the crack tip G can be expressed by the near crack tip integral only:

$$G=\lim_{\varepsilon\to 0}\left[\int_{\partial V_\varepsilon^o}t_i^o\frac{Du_i}{Da}\mathrm{d}\left(\partial V_\varepsilon^o\right)+\int_{V_\varepsilon^o}G_i^o\frac{Du_i}{Da}\mathrm{d}V_\varepsilon^o-\frac{\partial}{\partial D}\int_{V_\varepsilon^o}W\mathrm{d}V_\varepsilon^o\right] \cdots\cdots\cdots\cdots (15)$$

According to Atluri [59] and Okada and Atluri [41], equation (15) can be rewritten as

$$G=\lim_{\varepsilon\to 0}\left[\int_{\partial V_\varepsilon^o}\left(WN_1^\varepsilon-N_j^\varepsilon\pi_{ji}\frac{\partial u_i}{\partial X_1^o}\right)\mathrm{d}\left(\partial V_\varepsilon^o\right)\right]-\lim_{\varepsilon\to 0}\left[\int_{V_\varepsilon^o}G_i^o\frac{\partial u_i}{\partial X_1^o}\mathrm{d}V_\varepsilon^o\right]. \cdots\cdots (16)$$

The expressions for the strain energy density and the stresses in equations (2) and (6) are substituted into equation (16). One can reach the following expression:

$$G=\lim_{\varepsilon\to 0}\left[\int_{\partial V_\varepsilon^o}\left(W^{\mathrm{Mech}}N_1^\varepsilon-N_j^\varepsilon\pi_{ji}\frac{\partial u_i^{\mathrm{Mech}}}{\partial X_1^o}\right)\mathrm{d}\left(\partial V_\varepsilon^o\right)\right]$$
$$-\lim_{\varepsilon\to 0}\left[\int_{V_\varepsilon^o}G_i^o\frac{\partial u_i}{\partial X_1^o}\mathrm{d}V_\varepsilon^o\right]+\lim_{\varepsilon\to 0}\left[\int_{\partial V_\varepsilon^o}\left(W^{\mathrm{Prior}}N_1^\varepsilon-N_j^\varepsilon\pi_{ji}\frac{\partial u_i^{\mathrm{Prior}}}{\partial X_1^o}\right)\mathrm{d}\left(\partial V_\varepsilon^o\right)\right]$$
$$\cdots\cdots (17)$$

The terms in equation (17) associated with G_i^o, W^{Prior} and $\frac{\partial u_i^{\mathrm{Prior}}}{\partial X_1^o}$ vanish. This is because they have weaker singularities than the other terms. It is noted that in the derivations presented here the assumption of self-similar crack propagation must hold. For the concept of self-similar crack propagation, the readers are referred to Atluri [59].

Thus, we write the following expression, and let $\hat{G}$ denote the energy dissipation into the small but finite volume V_ε^o in the immediate vicinity of the crack tip, per unit crack extension:

$$\hat{G} = \int_{\partial V_\varepsilon^o} \left(W^{\mathrm{Mech}} N_1^\varepsilon - N_j^\varepsilon \pi_{ji} \frac{\partial u_i^{\mathrm{Mech}}}{\partial X_1^o} \right) \mathrm{d}\left(\partial V_\varepsilon^o \right) \cdots\cdots\cdots\cdots\cdots\cdots\cdots\cdots\cdots\cdots (18)$$

Here, the terms associated with G_i^o, W^{Prior}, and $\dfrac{\partial u_i^{\mathrm{Prior}}}{\partial X_1^o}$ are neglected because they are considered to be negligibly small. Hence, equation (18) expresses the energy dissipating into the small region V_ε^o in the immediate vicinity of the crack tip while the crack extends for a unit length.

We then introduce a function $q\left(\boldsymbol{X}^o \right)$ that is continuous and piecewise differentiable in the region $V_{Int.}^o - V_\varepsilon^o$ and equals zero at the outer surface of $V_{Int.}^o - V_\varepsilon^o$. Here, $V_{Int.}^o$ is a region surrounding the crack tip, as depicted in Figure 2(b). The term $q\left(\boldsymbol{X}^o \right)$ takes a constant value δ inside the small region V_ε^o, where δ is the amount of virtual crack extension at the crack tip. By applying the Gauss divergence theorem, a domain integral formulation is derived as:

$$\begin{aligned}
\hat{G}\delta &= \int_{\partial V_\varepsilon^o} \left(W^{\mathrm{Mech}} N_1^\varepsilon - N_j^\varepsilon \pi_{ji} \frac{\partial u_i^{\mathrm{Mech}}}{\partial X_1^o} \right) q \mathrm{d}\left(\partial V_\varepsilon^o \right) \\
&= -\int_{V_{Int.}^o - V_\varepsilon^o} \left(W^{\mathrm{Mech}} \delta_{j1} - \pi_{ji} \frac{\partial u_i^{\mathrm{Mech}}}{\partial X_1^o} \right) \frac{\partial q}{\partial X_j^o} \mathrm{d}\left(V_{Int.}^o - V_\varepsilon^o \right) \qquad \cdots\cdots\cdots (19) \\
&\quad -\int_{V_{Int.}^o - V_\varepsilon^o} \left(\frac{\partial W^{\mathrm{Mech}}}{\partial X_1^o} - \pi_{ji} \frac{\partial^2 u_i^{\mathrm{Mech}}}{\partial X_j^o \partial X_1^o} + G_i^o \frac{\partial u_i^{\mathrm{Mech}}}{\partial X_1^o} \right) q \mathrm{d}\left(V_{Int.}^o - V_\varepsilon^o \right)
\end{aligned}$$

It is noted that δ is often set to be unity.

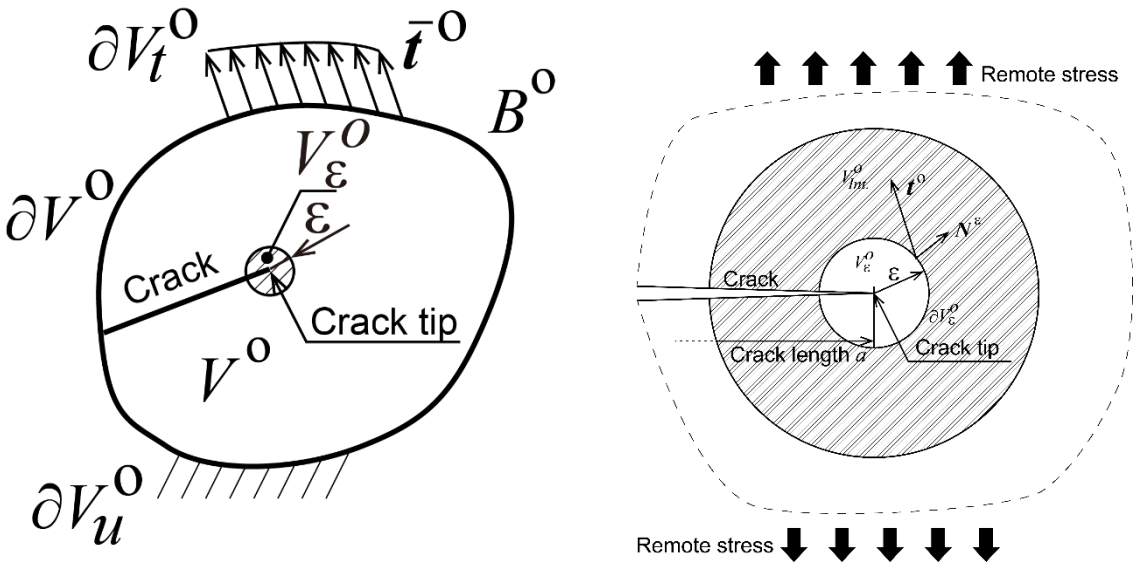

(a) Boundary value problem (b) Magnified view in the vicinity of the crack tip

Figure 2 Boundary value problem described in the original undeformed configuration B^o and its magnified view in the vicinity of the crack tip showing the small volume V_ε^o surrounding the crack tip and the integral domain $V_{Int.}^o$. [(a) Boundary value problem, and (b) Magnified view in the vicinity of the crack tip]

2.4 Expressions for the energy dissipation $\hat{G}$ in the three-dimensional problem

Following the discussions for the two-dimensional problem, a three-dimensional formulation is derived in this section. A part of the present derivation follows Arai, Okada, and Yusa [49, 50] for the three-dimensional J-integral. For the three-dimensional problem, similar discussions as those for the two-dimensional case are carried out. The domain V_ε^o inside a small cylinder of radius and length ε and b^o, respectively, as depicted in Figure 3, is considered. The volume V_ε^o is surrounded by the surface of the cylinder ∂V_ε^o and the end surfaces $\partial V_{\varepsilon-\mathrm{end}(+)}^o$ and $\partial V_{\varepsilon-\mathrm{end}(-)}^o$, as also shown in Figure 3.

$$
\begin{aligned}
Gb^o = & \int_{\partial V_t^o} \bar{t}_i^o \frac{Du_i}{Da} \mathrm{d}\left(\partial V_t^o\right) \\
& - \int_{\partial V_\varepsilon^o} t_i^o \frac{Du_i}{Da} \mathrm{d}\left(\partial V_\varepsilon^o\right) - \int_{\partial V_{\varepsilon-\mathrm{end}(+)}^o} t_i^o \frac{Du_i}{Da} \mathrm{d}\left(\partial V_{\varepsilon-\mathrm{end}(+)}^o\right) - \int_{\partial V_{\varepsilon-\mathrm{end}(-)}^o} t_i^o \frac{Du_i}{Da} \mathrm{d}\left(\partial V_{\varepsilon-\mathrm{end}(-)}^o\right) \\
& + \int_{V^o - V_\varepsilon^o} G_i^o \frac{Du_i}{Da} \mathrm{d}\left(V^o - V_\varepsilon^o\right) - \int_{V^o - V_\varepsilon^o} \pi_{ij} \frac{DF_{ji}}{Da} \mathrm{d}\left(V^o - V_\varepsilon^o\right) \\
& + \int_{\partial V_\varepsilon^o} t_i^o \frac{Du_i}{Da} \mathrm{d}\left(\partial V_\varepsilon^o\right) + \int_{\partial V_{\varepsilon-\mathrm{end}(+)}^o} t_i^o \frac{Du_i}{Da} \mathrm{d}\left(\partial V_{\varepsilon-\mathrm{end}(+)}^o\right) + \int_{\partial V_{\varepsilon-\mathrm{end}(-)}^o} t_i^o \frac{Du_i}{Da} \mathrm{d}\left(\partial V_{\varepsilon-\mathrm{end}(-)}^o\right) \\
& + \int_{V_\varepsilon^o} G_i^o \frac{Du_i}{Da} \mathrm{d}\left(V_\varepsilon^o\right) - \frac{D}{Da} \int_{V_\varepsilon^o} W \mathrm{d}V_\varepsilon^o
\end{aligned}
\quad \cdots\cdots (20)
$$

Here, V^o and ∂V_t^o are the volume of the body and the traction-described boundary, respectively. The notations are the same as the those for the two-dimensional problem. When the body is in equilibrium, equation (20) reduces to

$$
\begin{aligned}
Gb^o = & \int_{\partial V_\varepsilon^o} t_i^o \frac{Du_i}{Da} \mathrm{d}\left(\partial V_\varepsilon^o\right) + \int_{\partial V_{\varepsilon-\mathrm{end}(+)}^o} t_i^o \frac{Du_i}{Da} \mathrm{d}\left(\partial V_{\varepsilon-\mathrm{end}(+)}^o\right) + \int_{\partial V_{\varepsilon-\mathrm{end}(-)}^o} t_i^o \frac{Du_i}{Da} \mathrm{d}\left(\partial V_{\varepsilon-\mathrm{end}(-)}^o\right) \\
& + \int_{V_\varepsilon^o} G_i^o \frac{Du_i}{Da} \mathrm{d}\left(V_\varepsilon^o\right) - \frac{D}{Da} \int_{V_\varepsilon^o} W \mathrm{d}V_\varepsilon^o
\end{aligned}
\quad \cdots\cdots (21)
$$

As the volume $\bar{V}_\varepsilon^o$ in the vicinity of the crack front is considered to be very small, the terms having no and weak singularities can be neglected. Hence, in the same fashion as the two-dimensional formulation, energy $\hat{G}b^o$ dissipating into the small volume V_ε^o surrounding the crack front is given by the following expression:

$$
\begin{aligned}
\hat{G}b^o = & \int_{\partial V_\varepsilon^o} \left(W^{\mathrm{Mech}} N_1^\varepsilon - N_j^\varepsilon \pi_{ji} \frac{\partial u_i^{\mathrm{Mech}}}{\partial X_1^o} \right) \mathrm{d}\left(\partial V_\varepsilon^o\right) \\
& - \left[\int_{\partial V_{\varepsilon-\mathrm{end}(+)}^o} N_j^\varepsilon \pi_{ji} \frac{\partial u_i^{\mathrm{Mech}}}{\partial X_1^o} \mathrm{d}\left(\partial V_{\varepsilon-\mathrm{end}(+)}^o\right) - \int_{\partial V_{\varepsilon-\mathrm{end}(-)}^o} N_j^\varepsilon \pi_{ji} \frac{\partial u_i^{\mathrm{Mech}}}{\partial X_1^o} \mathrm{d}\left(\partial V_{\varepsilon-\mathrm{end}(-)}^o\right) \right]
\end{aligned}
\quad \cdots\cdots (22)
$$

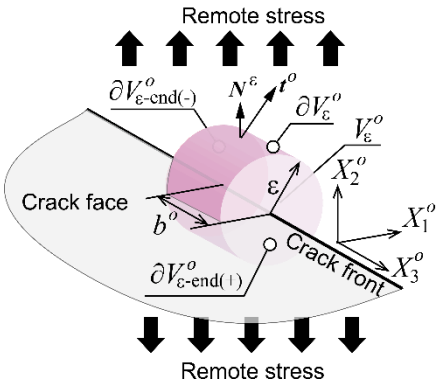

Figure 3 Infinitesimally small volume V^o_ε and its boundaries ∂V^o_ε, $\partial V^o_{\varepsilon\text{-end}(+)}$, and $\partial V^o_{\varepsilon\text{-end}(-)}$.

Then, following Arai et al. [49, 50], the length b^o of the small pipe is set to be zero in the limit. The first integral in the above equation degenerates to the contour integral at the periphery ∂A^o_ε of a small disk A^o_ε, as illustrated in Figure 4. The second and third integrals reduce to the area integral inside A^o_ε. Its integrand is the derivative of $\pi_{3i}\dfrac{\partial u_i^{\text{Mech}}}{\partial X_1^o}$ with respect to the coordinate X_3^o, which is in the tangential direction of the crack front curve. We can write the following expression:

$$\hat{G}=\int_{\partial A^o_\varepsilon}\left(W^{\text{Mech}}N_1^\varepsilon-N_j^\varepsilon\pi_{ji}\frac{\partial u_i^{\text{Mech}}}{\partial X_1^o}\right)\mathrm{d}\left(\partial A^o_\varepsilon\right)-\int_{A^o_\varepsilon}\frac{\partial}{\partial X_3^o}\left(\pi_{3i}\frac{\partial u_i^{\text{Mech}}}{\partial X_1^o}\right)\mathrm{d}A^o_\varepsilon \quad (23)$$

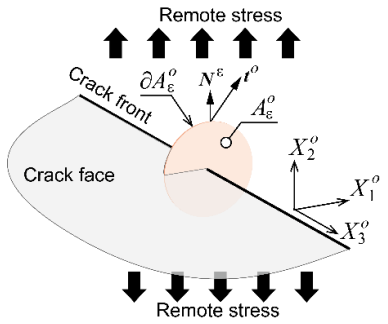

Figure 4 Degenerated disk A^o_ε by setting the length b^o of small volume V^o_ε to be

zero in the limit.

Then, a function $q\left(\boldsymbol{X}^o\right)$ is introduced. Here, $q\left(\boldsymbol{X}^o\right)$ is a function of X_3^o in the small volume Ω_ε^o and is set to be zero at both ends of Ω_ε^o. The length along the crack front line and radius of the volume Ω_ε^o are Δ and ε, respectively, as shown in Figure 5. After $q\left(\boldsymbol{X}^o\right)$ is multiplied to both sides of equation (23), they are integrated for length Δ along the crack front. We obtain the following expression:

$$\hat{G}=\frac{1}{\Delta A}\int_{\partial\Omega_\varepsilon^o}\left(W^{\mathrm{Mech}}N_1^\varepsilon-N_j^\varepsilon\pi_{ji}\frac{\partial u_i^{\mathrm{Mech}}}{\partial X_1^o}\right)q\left(X_3^o\right)\mathrm{d}\left(\partial\Omega_\varepsilon^o\right) \\ -\frac{1}{\Delta A}\int_\Delta\int_{A_\varepsilon^o}\frac{\partial}{\partial X_3^o}\left(\pi_{3i}\frac{\partial u_i^{\mathrm{Mech}}}{\partial X_1^o}\right)q\left(X_3^o\right)\mathrm{d}A_\varepsilon^o\mathrm{d}X_3^o \quad \cdots\cdots\cdots\cdots\cdots\cdots (24)$$

Here, ΔA is the area of virtual crack extension ($\Delta A=\int_\Delta q\mathrm{d}X_3^o$), and $\partial\Omega_\varepsilon^o$ is the surface of the cylindrical volume Ω_ε^o of radius and length ε and Δ, respectively. The second integral in the right-hand side of equation (24) can be converted to a simpler form after integrating by parts:

$$\int_\Delta\int_{A_\varepsilon^o}\frac{\partial}{\partial X_3^o}\left(\pi_{3i}\frac{\partial u_i^{\mathrm{Mech}}}{\partial X_1^o}\right)q\left(X_3^o\right)\mathrm{d}A_\varepsilon^o\mathrm{d}X_3^o=-\int_{\Omega_\varepsilon^o}\pi_{3i}\frac{\partial u_i^{\mathrm{Mech}}}{\partial X_1^o}\frac{\partial q\left(X_3^o\right)}{\partial X_3^o}\mathrm{d}\Omega_\varepsilon^o \quad \cdots (25)$$

Finally, we extend the definition of the function $q\left(\boldsymbol{X}^o\right)$ such that it is a continuous and piecewise-differentiable positive function in the domain Ω_{Int}^o. Then, $q\left(\boldsymbol{X}^o\right)$ is set to be zero at the outer surface $\partial\Omega_{Int}^o$ and outside the domain Ω_{Int}^o. Then, by applying the Gauss divergence theorem, a domain integral expression is derived. It is noted that Ω_{Int}^o

contains the domain Ω_ε^o inside of it. Finally, the energy dissipating into a small cylindrical region of radius and length ε and unity, respectively, can be expressed by the domain integral formulation. Then, we redefine the three-dimensional J-integral in a domain integral expression as

$$J = \hat{G} = -\frac{1}{\Delta A}\int_{\Omega_{Int}^o}\left(W^{\text{Mech}}\delta_{1j} - \pi_{ji}\frac{\partial u_i^{\text{Mech}}}{\partial X_1^o}\right)\frac{\partial q}{\partial X_j^o}\,\mathrm{d}\Omega_{Int}^o - \frac{1}{\Delta A}\int_{\Omega_{Int}^o-\Omega_\varepsilon^o}\left(\frac{\partial W^{\text{Mech}}}{\partial X_j^o} - \pi_{ji}\frac{\partial^2 u_i^{\text{Mech}}}{\partial X_j^o \partial X_1^o}\right)q\,\mathrm{d}\left(\Omega_{Int}^o - \Omega_\varepsilon^o\right) \quad \cdots\cdots (26)$$

The three-dimensional J-integral as redefined in equation (26) has a mean of rigorous extension of two-dimensional T_ε^* of Okada and Atluri [41]. Thus, we may name it to be $T_\varepsilon^{*3\text{D}}$ which is the three-dimensional version of T_ε^*.

As stated earlier, the material is not assumed to be homogeneous in the derivation of equation (26). The mechanical properties of the material may vary continuously. It is also noted that for the absence of prior deformation that equation (26) degenerates to the expression of the J-integral without the residual stresses. The formulation degenerates to the J-integral formulation as presented by Arai et al. [49, 50] as

$$J = \hat{G} = -\frac{1}{\Delta A}\int_{\Omega_{Int}^o}\left(W\delta_{1j} - \pi_{ji}\frac{\partial u_i}{\partial X_1^o}\right)\frac{\partial q}{\partial X_j^o}\,\mathrm{d}\Omega_{Int}^o - \frac{1}{\Delta A}\int_{\Omega_{Int}^o-\Omega_\varepsilon^o}\left(\frac{\partial W}{\partial X_j^o} - \pi_{ji}\frac{\partial^2 u_i}{\partial X_j^o \partial X_1^o}\right)q\,\mathrm{d}\left(\Omega_{Int}^o - \Omega_\varepsilon^o\right) \quad \cdots\cdots (27)$$

It is noted that when a hyper-elastic material is assumed, the second integral of equation (27) vanishes. The formulation degenerates to the case of classical J-integral formulation by the domain integral representation.

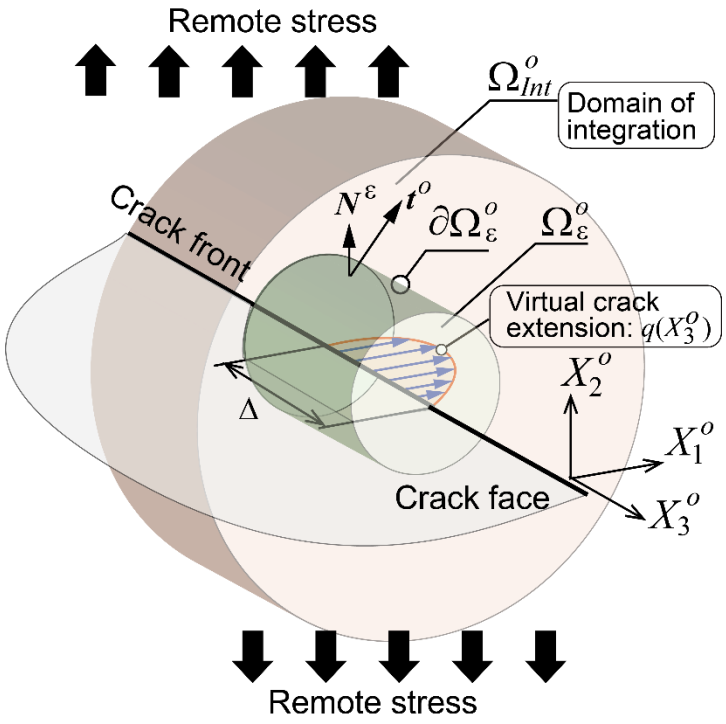

Figure 5 Integral domain $\Omega^o_{Int.}$ surrounding the crack front and the virtual crack extension $q\left(\boldsymbol{X}^o\right)$.

2.5 Variation of the function $q\left(\boldsymbol{X}^o\right)$ and the spatial derivatives of the strain energy density and the displacement gradients

According to the discussions in the preceding sections, the function $q\left(\boldsymbol{X}^o\right)$ is assigned as follows. The cross section of the integral domain $\Omega^o_{Int.}$ is depicted in Figure 6(a). Then, the integral domain is defined by rotating the cross section about the crack front. The outer shape of the integral domain is depicted in Figure 6(b). The section of the small cylindrical region Ω^o_ε of length and radius Δ and ε, respectively, is also presented in Figure 6(a). The function $q\left(\boldsymbol{X}^o\right)$ varies in the direction of the crack front direction X^o_3 only, inside the small cylindrical region Ω^o_ε. Moreover, $q\left(\boldsymbol{X}^o\right)$ is unity at the center

and is zero at both ends of the segment Δ. The outer radius of the integral domain $\Omega^o_{Int.}$ is denoted by r^o. The width of the integral domain at the outer radius r^o is denoted by w^o. Here, r^o and w^o are presented in Figure 6(a). The term w^o is larger than or equal to Δ. The magnitude of the function $q\left(\boldsymbol{X}^o\right)$ linearly decreases from the outer surface of $\partial\Omega^o_\varepsilon$ to zero at the outer radius r^o of $\Omega^o_{Int.}$. The variation of $q\left(\boldsymbol{X}^o\right)$ is schematically illustrated in Figure 6(a). When w^o is larger than Δ, there is a plateau of length $w^o - \Delta$ at the center of the section of the integral domain.

The values of $q\left(\boldsymbol{X}^o\right)$ are assigned to the convex nodes of the finite element model, as discussed in Okada and Ohata [60], when the nodes are inside the integral domain $\Omega^o_{Int.}$. For the nodes outside of $\Omega^o_{Int.}$, their values of the function are set to be zero. The values of $q\left(\boldsymbol{X}^o\right)$ at the mid-nodes are assigned by averaging those at the convex nodes. Then, $q\left(\boldsymbol{X}^o\right)$ inside each element is expressed using the shape functions of the element. Hence, the domain integrals of equations (26) and (27) are carried out using the Gauss quadrature performed on the finite elements. The integration is performed on all elements that have non-zero $q\left(\boldsymbol{X}^o\right)$ values at their nodes. It is noted that the integral domain based on the elements may have an angular shape, as presented by Okada and Ohata [60]. The readers are referred to [60] for complete descriptions of the integral domain.

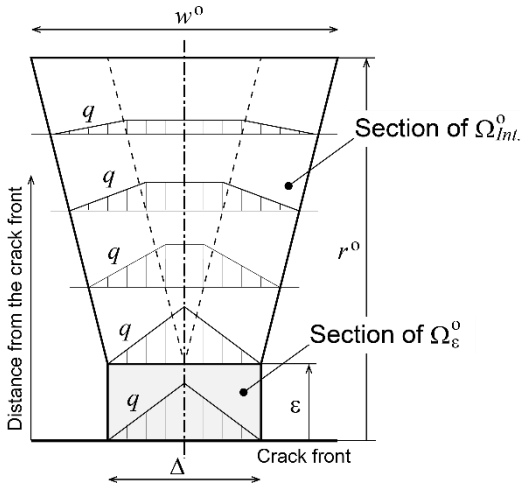

(a) Section and variation of the ~~virtual crack extension~~ function (q)

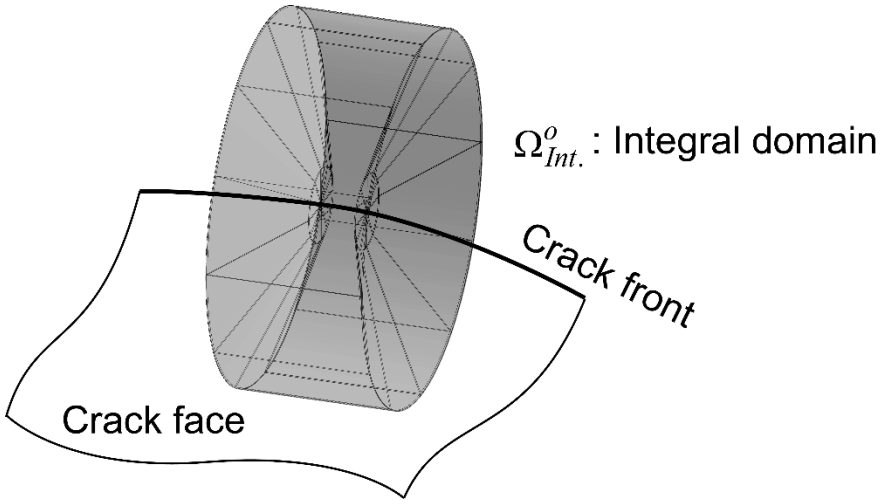

(b) Outer shape of the integral domain $\Omega^o_{Int.}$

Figure 6 Schematic illustrations of the section and the outer shape of the integral domain $\Omega^o_{Int.}$. The variation of function q is also illustrated. [(a) Section and variation of the function (q), and (b) Outer shape of the integral domain $\Omega^o_{Int.}$]

For the evaluations of the derivatives of the strain energy density and the displacements gradients in the second integrals of equations (26) and (27), the method proposed by Koshima and Okada [46] is adopted. It assigns values to the nodes using the superconvergent patch recovery method of Zienkiewicz and Zhu [47, 48]. Then, the shape functions of the finite elements are used for the computations of the derivatives. Further

details are described in Koshima and Okada [46].

3. Numerical examples for the problems with residual stresses and with spatially varying mechanical properties of a material

All the numerical analyses that are presented in this paper were carried out using MSC.Marc 2016 [61]. The J-integral evaluations were performed by an in-house software developed by the authors. The finite element analysis results were passed to the in-house software through the t19 post process file supported by MSC.Marc 2016 [61]. The t19 file is in a text format, and the data was therefore easily exported to the software.

3.1 Example problem for structures with residual stresses: A plate subject to a bending moment followed by tension (A crack in a plate after spring back)

In this section, an example problem for the J-integral evaluation under residual stresses is presented. The finite element analyses were performed by MSC.Marc 2016 [61]. A plate made of a mild steel was assumed. Young's modulus, Poisson's ratio, and the yield stress were set to be 206 GPa, 0.3, and 300 MPa, respectively. The linear isotropic hardening J-2 plasticity with the hardening modulus 0.3 MPa was assumed. The plate was subject to a gradually increasing applied moment at its end surface, which was released, as shown in Figure 7(a). The maximum value of the applied moment was 2.75 N m. Hence, residual stresses remained in the body. The residual stress data was stored in the "t19" post process file supported by MSC.Marc 2016. The magnitude of deformation due to the bending moment and the spring back were assumed to be small. Therefore, the deformation was neglected. Then, the residual stress data was introduced from the post process file to the original undeformed finite element model for the problem of plate with a crack. A semi-circular surface flaw, the depth of which was half of the plate thickness, was assumed. Finally, the plate was subject to a tensile deformation, as depicted in Figure 7(b). A prescribed displacement was applied to the top surface of the plate. Its maximum value was 0.15 mm. The same finite element model was used for both the plate bending and tension problems. The double nodes were placed on the crack face. They shared the same degrees of freedom as the multiple point constraints while the bending moment was applied and released. Then, the constraints were deleted, generating the crack face. Although the crack face may have closed due to the compressive residual stress, we did not assign a contact condition to the crack face for the simplicity of the analysis. The finite element model is shown in Figure 8. Figures 8(a), 8(b), and 8(c) show an overall view of the finite element model, a magnified view of the surface point of the crack, and

the crack face, respectively.

The deformation and the distribution of the equivalent plastic strain are depicted in Figure 9(a) after the plate was subject to the applied moment. The distribution of the residual stress (σ_{33}) is depicted in Figure 9(b). The figures show the central section and the surface of the plate. In Figure 10, the variation of the residual stress along a line connecting both surfaces of the plate at the central section is depicted. The solid line presents the results computed by the Euler-Bernoulli beam theory assuming one-dimensional elastic-perfect plasticity. The values of residual stresses predicted by the finite element analysis and by the beam theory are very similar.

Then, the plate with the semi-circular crack was subject to the tensile deformation, as depicted in Figure 7(b). Figure 11 presents the load-displacement curve while the plate was subject to the tensile deformation. It indicates that the plate has undergone a considerable amount of plastic deformation. The deformation and the distribution of the equivalent plastic strain are presented in Figure 12. Figure 12 is the magnified view in the vicinity of the crack. The surface and the central section of the plate are shown. It is seen that the crack mouth opened largely and that the plastic deformation accumulated in the vicinity of the crack front. A band having a relatively large magnitude of plastic strain is seen, indicating the formation of a shear band.

J-integral evaluations were performed using three different sizes of integral domains. Their examples are depicted in Figures 13(a), 13(b), and 13(c) for small, medium, and large integral domains, respectively. Their representative outer radius r^o is 10, 18, or 25 times the width (0.03 mm) of elements along the crack front. They are 0.3 mm, 0.54 mm, and 0.75 mm, respectively. The representative width Δ of the integral domain along the crack front is 14 times the crack front element length. The value of w^o at the outer radius is 22 times the element size along the crack front. Here, Δ and w^o are 0.42 mm and 0.66 mm, respectively. The details of how the integral domain is set up are described by Okada and Ohata [60]. The radius ε of the inner region Ω_ε^o was set to be three times of the element width along the crack front. That is 0.09 mm. The region of Ω_ε^o is indicated

by red in the figures.

In Figure 14(a), the results of the J-integral evaluations are presented. The distributions of the evaluated J-integral values when the magnitude of the tensile deformation was relatively small are presented. The applied displacement was 0.02 mm. In this case, due to the residual stresses, the results of the J-integral evaluation by its first integral of equation (27) strongly depend on the radii of the integral domains. When the second integral of equation (27) was included in the evaluation, the dependencies on the radii of the integral domain disappeared. It can be considered that the magnitudes of the residual stresses were greater than those of the stresses that were induced by the applied loads. In Figure 14(b), the results of the J-integral evaluations when the crack opened largely are presented. In this case, the dependencies of the first integral on the radius of the integral domain were somewhat reduced.

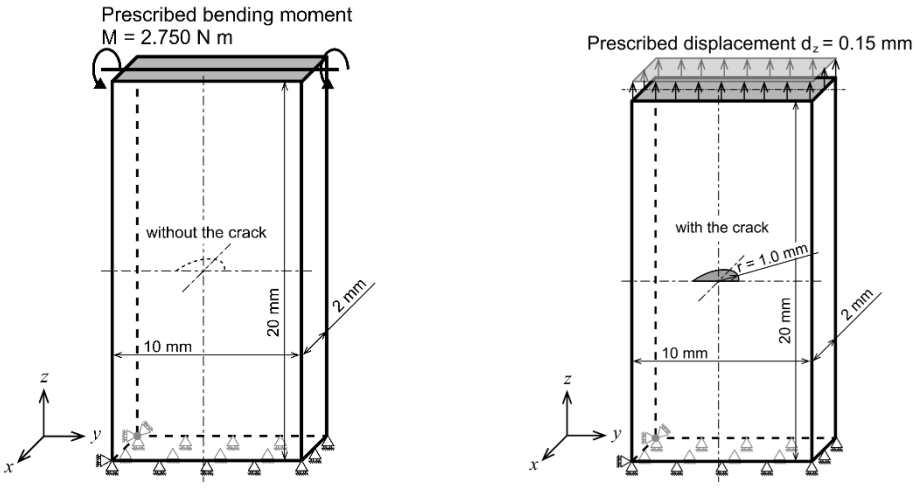

(a) Plate without a crack is subject to a bending moment

(b) Plate with a crack is subject to tensile deformation

Figure 7 Schematic presentations of a plate subject to elastic-plastic deformation under an applied moment, producing residual stresses. Then, a semi-circular crack of radius is 1.0 mm is assumed, and the plate is subject to a large elastic-plastic deformation under an applied tensile load. [(a) Plate without a crack is subject to a bending moment, and (b) Plate with a crack is subject to tensile deformation]

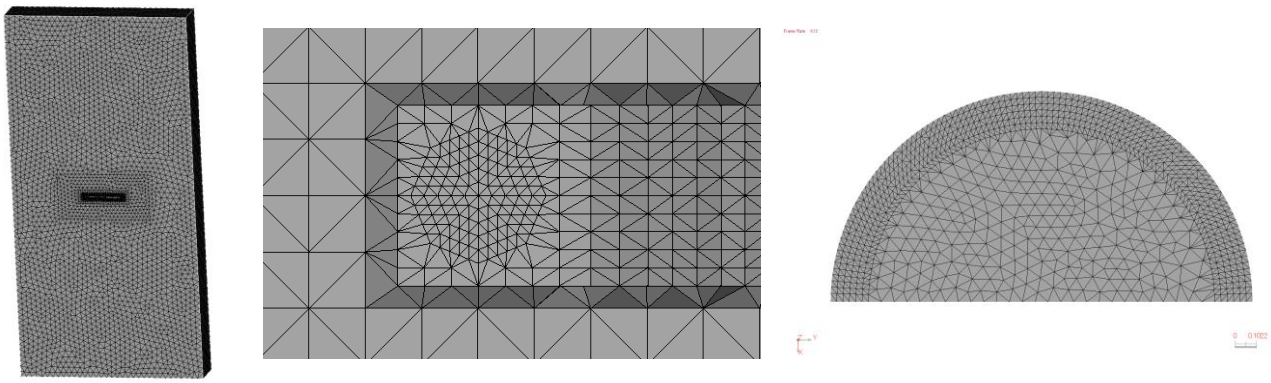

(a) Overall model (b) Cross section near the crack tip (c) Crack plane

Figure 8 Finite element model for the plate subject to a bending moment and a tensile load. [(a) Overall model, (b) Cross section near the crack tip, and (c) Crack plane]

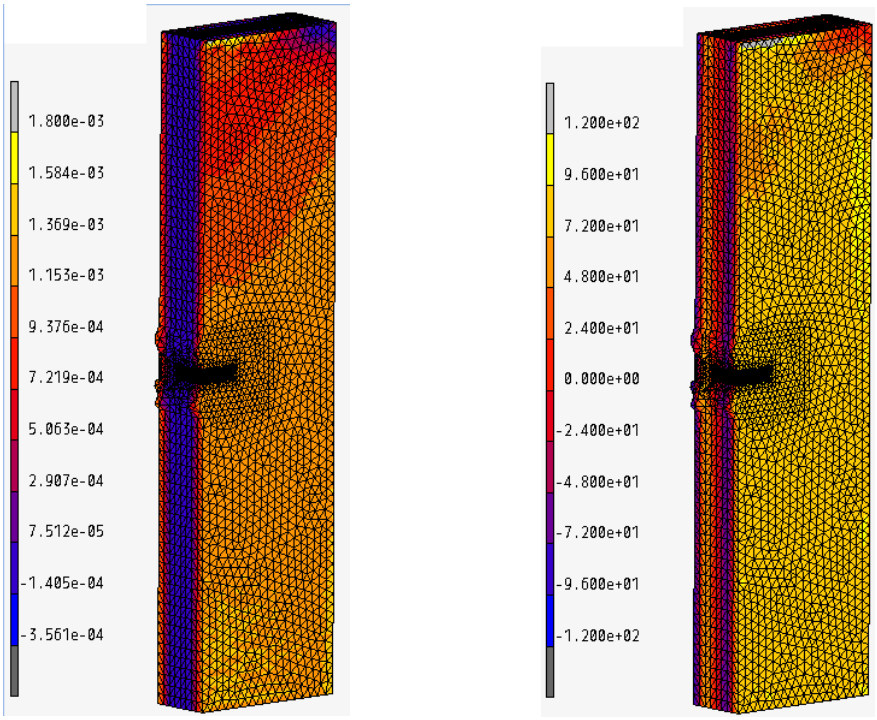

(a) Equivalent plastic strain (b) Stress σ_{zz}

Figure 9 Distributions of equivalent plastic strain and stress σ_{zz} after bending and spring back. [(a) Equivalent plastic strain, and (b) Stress σ_{zz}]

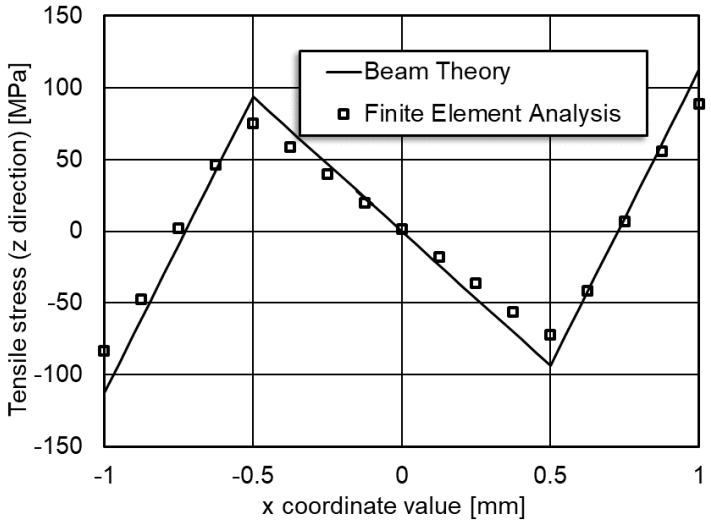

Figure 10 Comparison between the distributions of the residual stress σ_{zz} in the x-direction at the center of the plate, that computed under the assumption of the Euler-Bernoulli beam theory, and that evaluated by the present finite element analysis.

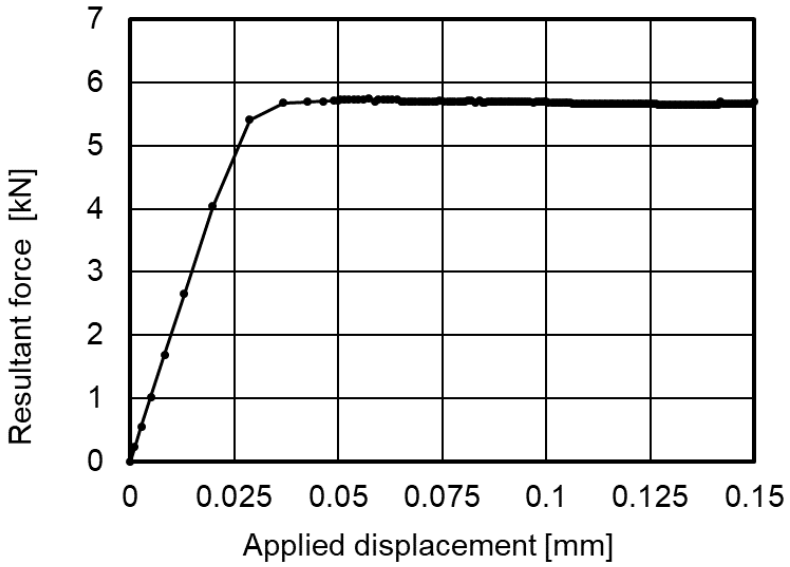

Figure 11 Load-displacement curve when the plate was subject to a tensile load.

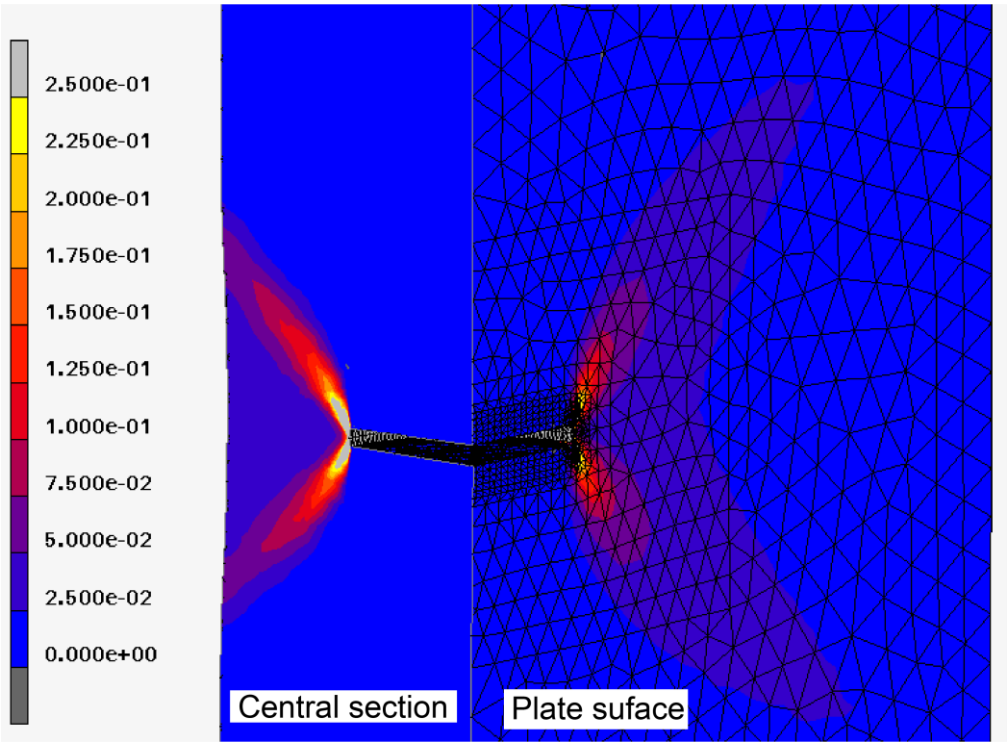

Figure 12 Distribution of equivalent plastic strain at $U_z = 0.15$ mm.

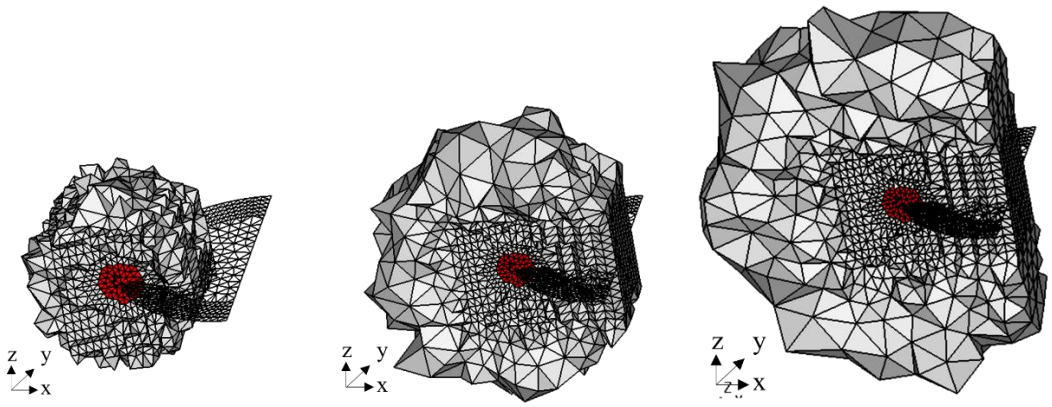

(a) $r^o = 0.30$ mm (small) (b) $r^o = 0.54$ mm (medium) (c) $r^o = 0.75$ mm (large)

Figure 13 Examples of integral domains having radii r^o of the integral domain $\Omega^o_{Int.}$ of (a) 0.30 mm, (b) 0.54 mm, and (c) 0.75 mm. They are designated to be small, medium, and large integral domains, respectively. [(a) $r^o = 0.30$ mm (small), (b) $r^o = 0.54$ mm (medium), and (c) $r^o = 0.75$ mm (large)]

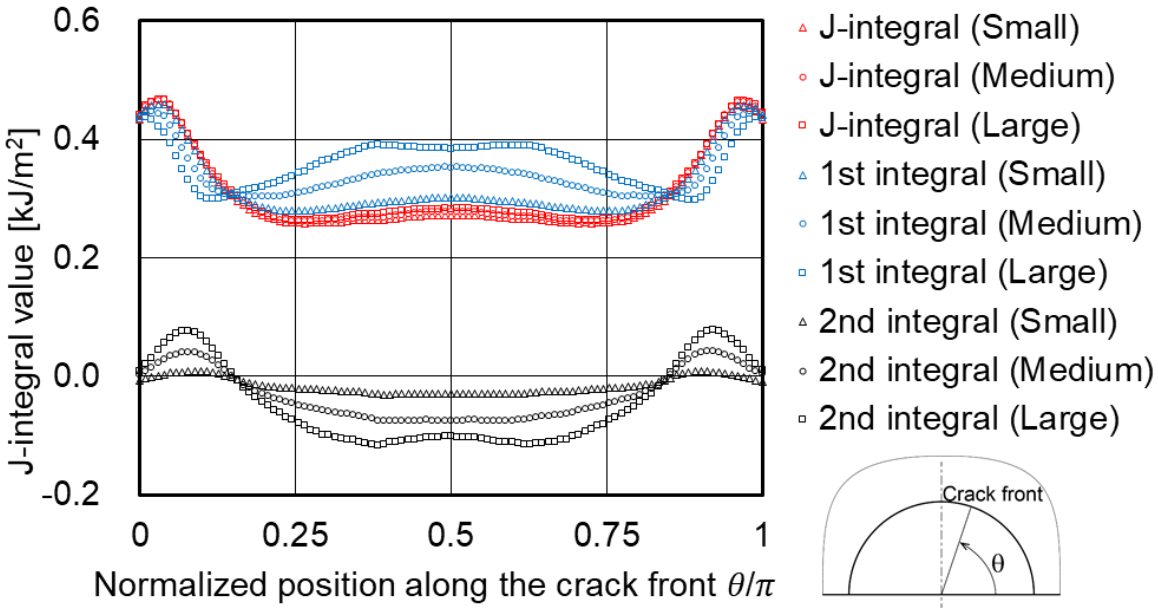

(a) Applied displacement 0.02 mm

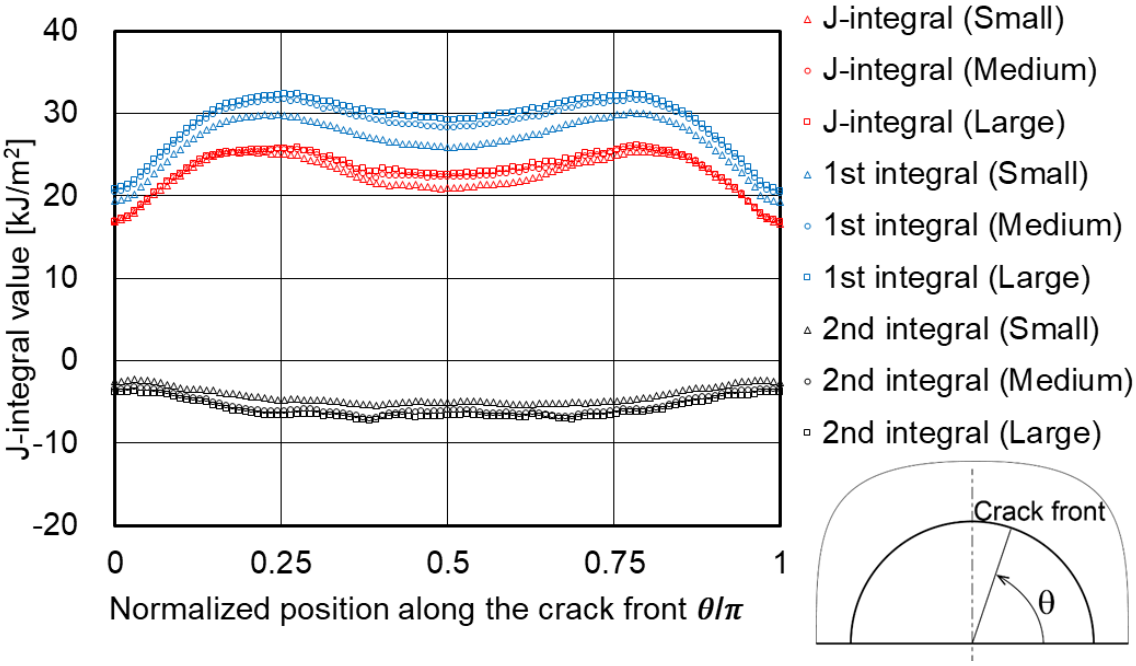

(b) Applied displacement 0.150 mm

Figure 14 Distributions of the evaluated J-integral values by the present formulation. [(a) Applied displacement: 0.02 mm, and (b) Applied displacement: 0.150 mm]

3.2 Example problem for structures with residual stresses: A plate with a hole subject to cold work

A cold work operation of enlarging a hole in a plate is considered in this section. During this cold work operation, a compressive residual stress at the periphery of the hole develops. The thickness of the plate and the radius of the hole were set up according to Pavier [11].

A plate having a length, width, and thickness of 120 mm, 100 mm, and 6 mm was assumed, as depicted in Figure 15(a). An aluminum alloy was assumed. Young's modulus and Poisson's ratios were set to be 71.6 GPa and 0.28, respectively. The initial yield stress was 320 MPa, and a linear strain hardening law was adopted. The hardening modulus was set to be 0.33 MPa, which is a very small value. A circular hole having a radius of 3.175 mm was placed at the center of the plate, as shown in Figure 15(b). The circular hole was expanded by the applied radial displacement at its surface. The magnitude of the displacement was 4% of its radius, as also illustrated in Figure 15(b). After the circular hole was expanded, the surface of the hole was set to be free from the surface traction. The residual stresses were generated by the cold work. It is noted that the circumferential residual stress was especially large. Then, two through cracks of length 1.588 mm were introduced at the hole edge. Due to the circumferential compressive residual stress, the crack face closes. Thus, a contact condition was set on the crack face. Following the introduction of the crack, the plate was subject to the tensile deformation. The top face of the plate was subject to the prescribed displacement, as illustrated in Figure 15(c). Due to the symmetry of the problem, 1/4 of the plate was considered. The value of the prescribed displacement was gradually increased, and its final value was set to be 0.5 mm. In Figure 16, the finite element model that was used for both analyses is presented. There are a total of 256,775 nodes and 183,058 quadratic tetrahedral finite elements. The element width along the crack front was set to be 0.126 mm.

In Figure 17, the variations of the radial and circumferential residual stress components with respect to the distance from the hole surface are depicted. In Figure 17, they are normalized by the value of the initial yield stress. It is seen that a large magnitude of circumferential residual stress at the hole surface developed due to the cold work, especially at the mid-thickness.

Then, the plate was subjected to tensile deformation. The load-displacement relation is plotted in Figure 18. The load-displacement curve indicates that the plate underwent a significant amount of nonlinear deformation. The deformation and the accumulation of equivalent plastic strain in the vicinity of the crack are shown in Figure 19. As seen in the

figure, the crack mouth opened largely, and the material in the vicinity of the crack front experienced a large magnitude of plastic deformation.

The J-integral evaluations were performed. Three different sizes of integral domains were set. Their representative sizes were set such that width Δ at the crack front was 0.38 mm, which was three times the element size (0.126 mm) at the crack front. The width w^o at the outer radius r^o was set to be 0.76 mm, which was six times the element size. The radius r^o was 1.9 mm, 3.8 mm, or and 5.7 mm, which were, respectively, 15, 30, and 45 times the element size. The radius ε of the small volume Ω_ε^o was set to be 0.5 mm, which was approximately three times the element size. Examples of the integral domains are shown in Figure 20. They are designated to be small, medium, and large integral domains.

In Figure 21(a), the variations of the J-integral values when the applied displacement was 0.2 mm are depicted. The values of the J-integrals evaluated by the first integral only are found to be strongly dependent on the radius of the integral domain. However, the total of the first and second integrals appears to be independent of the radius of the integral domain.

The results of J-integral evaluations when the applied displacement was 0.5 mm are depicted in Figure 21(b). In this case, the results of the computations using the first integral only are seen to be less dependent on the radius of the integral domain compared with those presented in Figure 21(a). It can be considered that the magnitudes of the strains due to the applied displacement dominate those of elastic strains due to the residual stresses. The totals of the first and second integrals appear to be independent of the radius of the integral domain. It can be summarized that the results of the proposed J-integral evaluations are seen to be independent of the radius of the integral domain by the inclusion of the second integral.

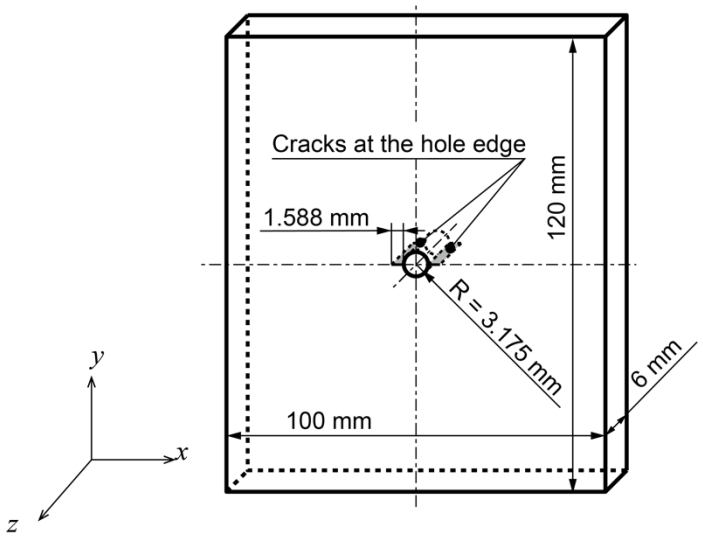

(a) Geometries of the plate, the hole and the crack

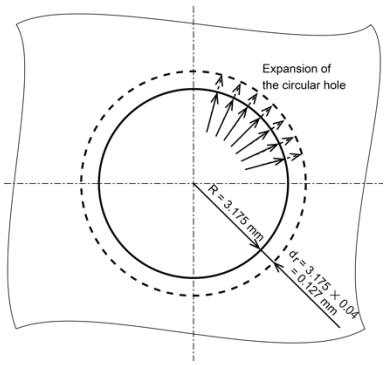

(b) Problem of cold work

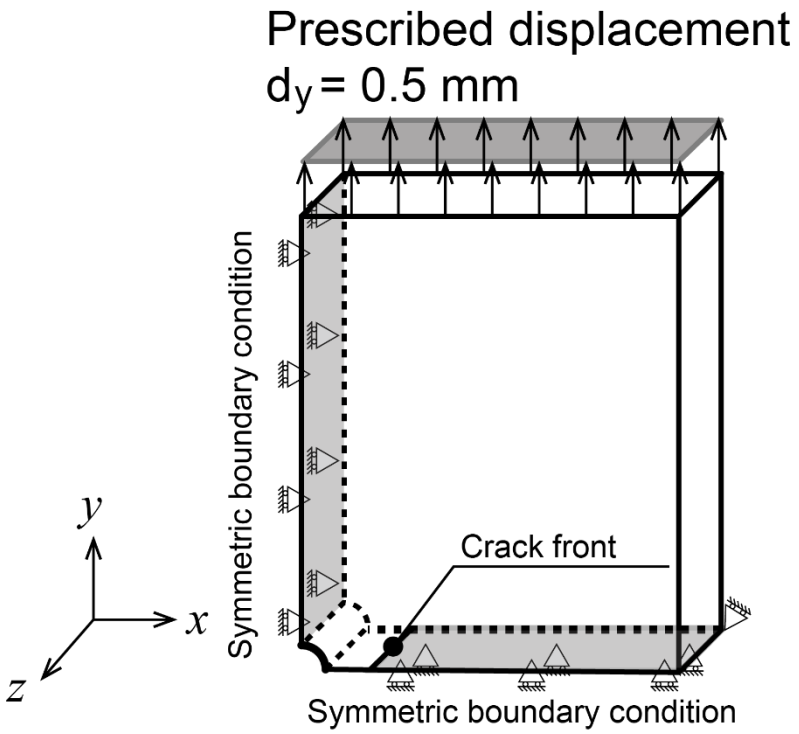

(c) Plate with a circular hole subject to a tensile load

Figure 15 Schematic diagram of the problem of cold working of a circular hole in a flat plate. Then, a through crack is assumed at the edge of the hole, and the plate is subject to a tensile load. [(a) Geometries of the plate, the hole, and the crack, (b) Problem of cold work, and (c) Plate with a circular hole subject to a tensile load]

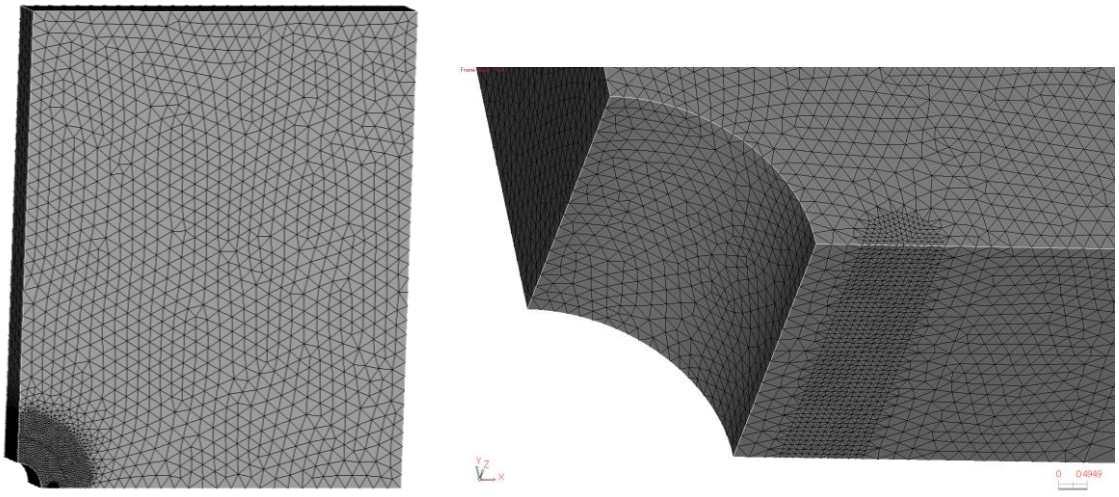

Figure 16 Finite element model for the problem of cold work, followed by tensile deformation.

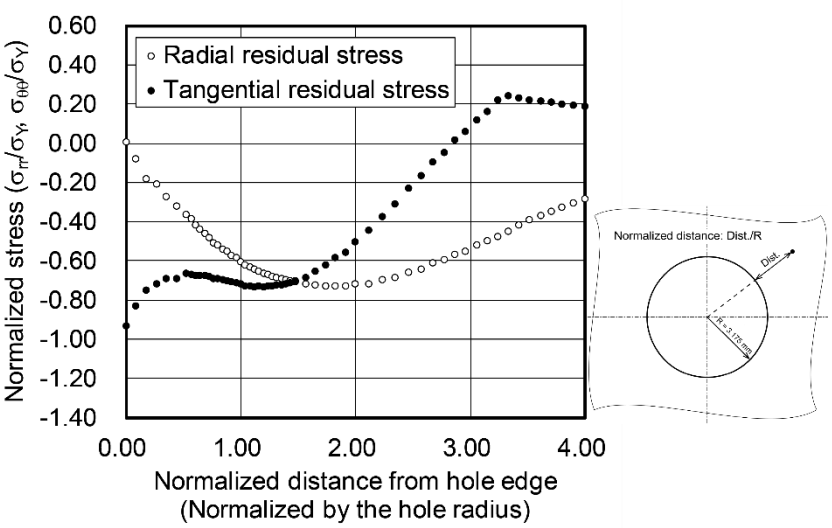

(a) At the surface

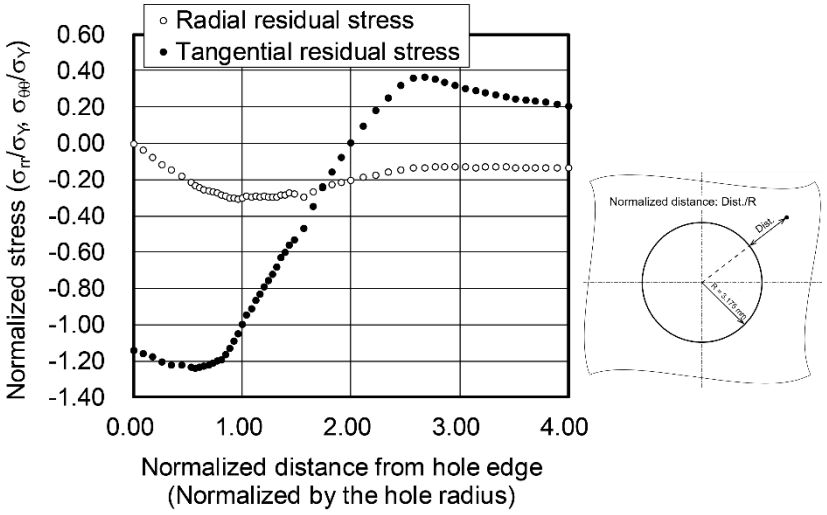

(b) At the mid-thickness

Figure 17 Variations of the residual stresses with respect to the distance from the hole edge at the surface and at the mid-thickness. [(a) At the surface, and (b) At the mid-thickness]

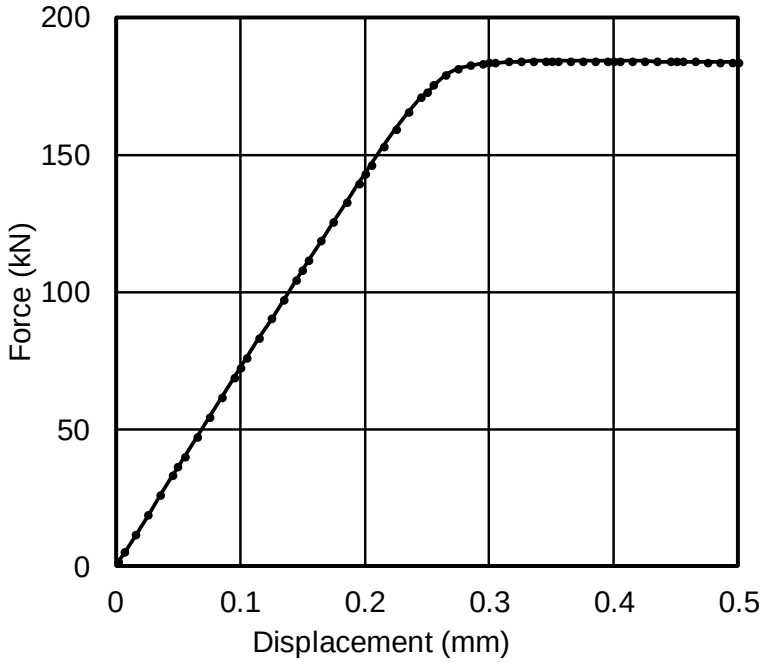

Figure 18 Relationship between the resultant force and the applied vertical displacement.

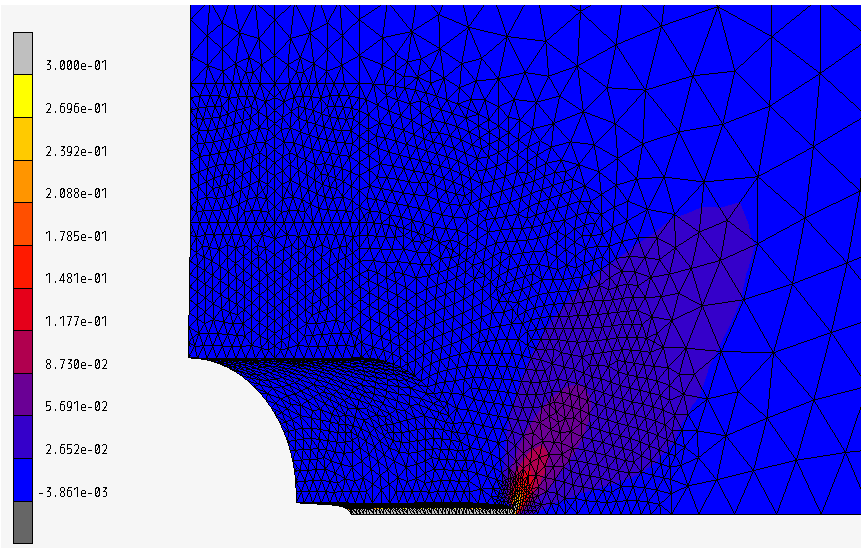

Figure 19 Distribution of equivalent plastic strain when the applied displacement is 0.5 mm.

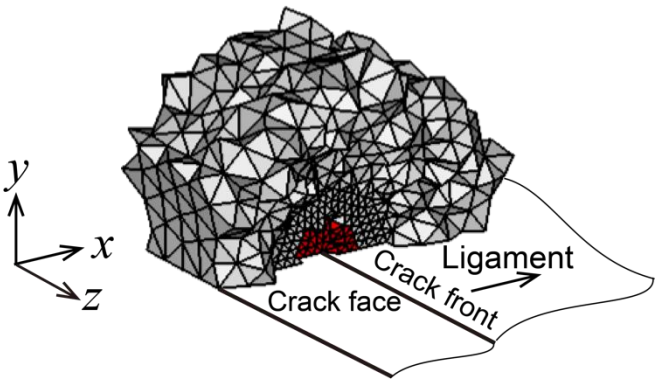

(a) r^o = 1.9 mm

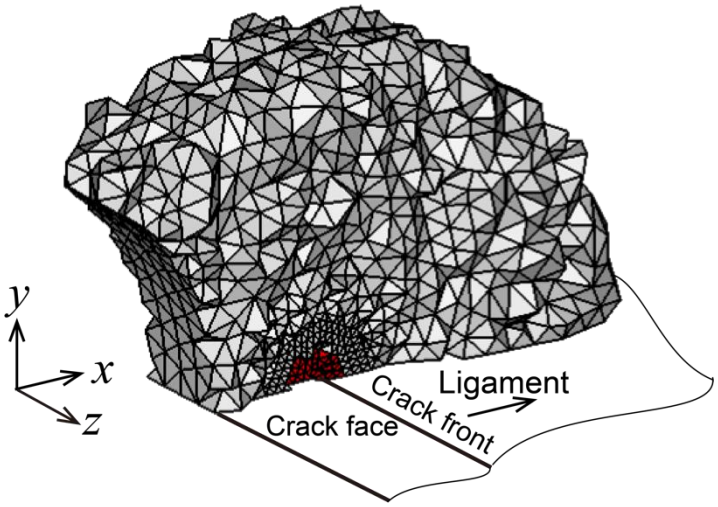

(b) r^o = 3.8 mm

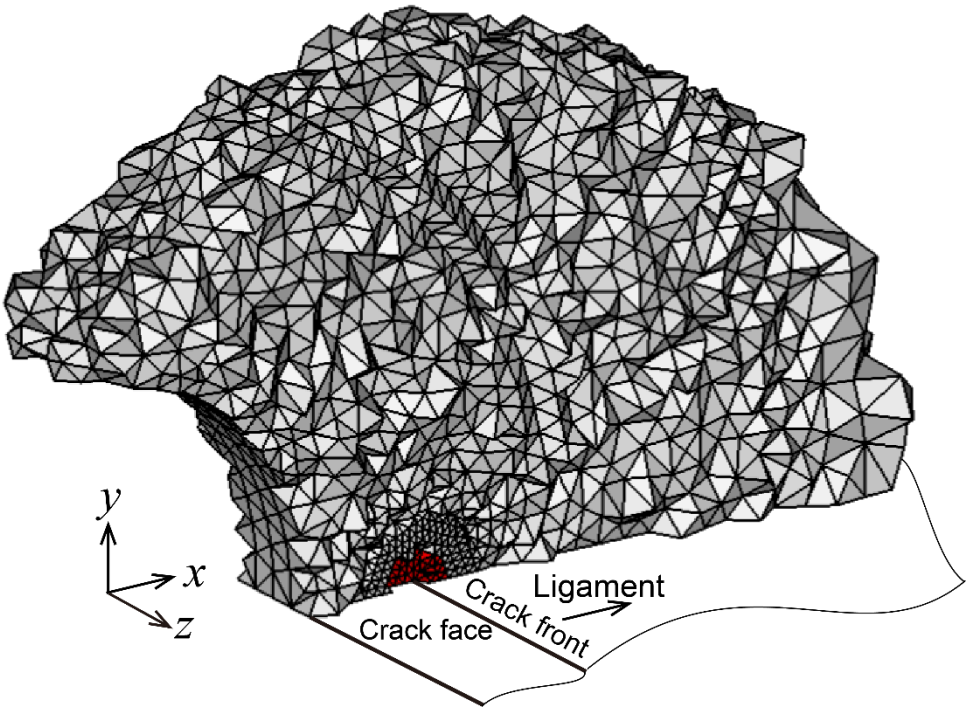

(c) r^o = 5.7 mm

Figure 20 Examples of the integral domains for the problem of cold working followed by the tensile deformation. The radius ε of the inner region Ω_ε^o is 0.5 mm. [(a) r^o = 1.9 mm, (b) r^o = 3.8 mm, and (c) r^o = 5.7 mm]

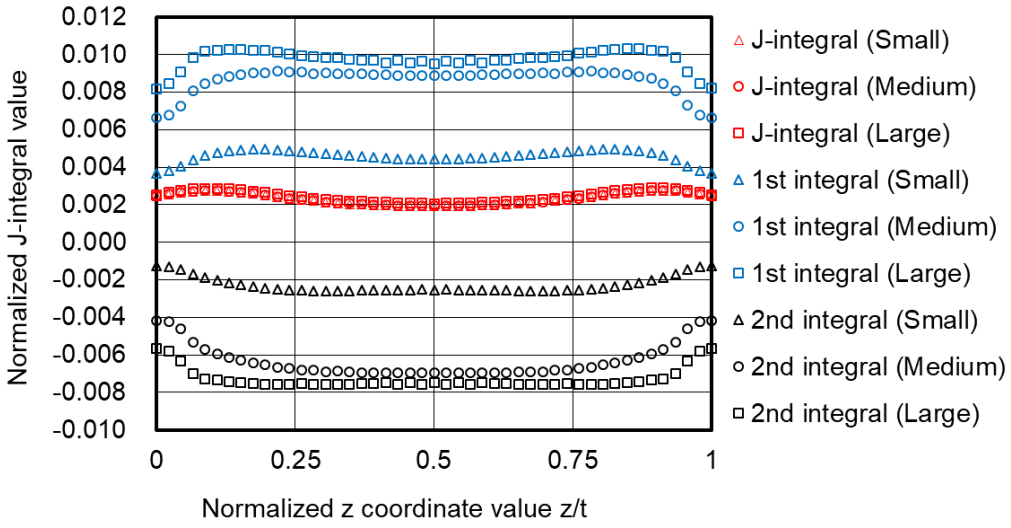

(a) Applied displacement 0.20 mm

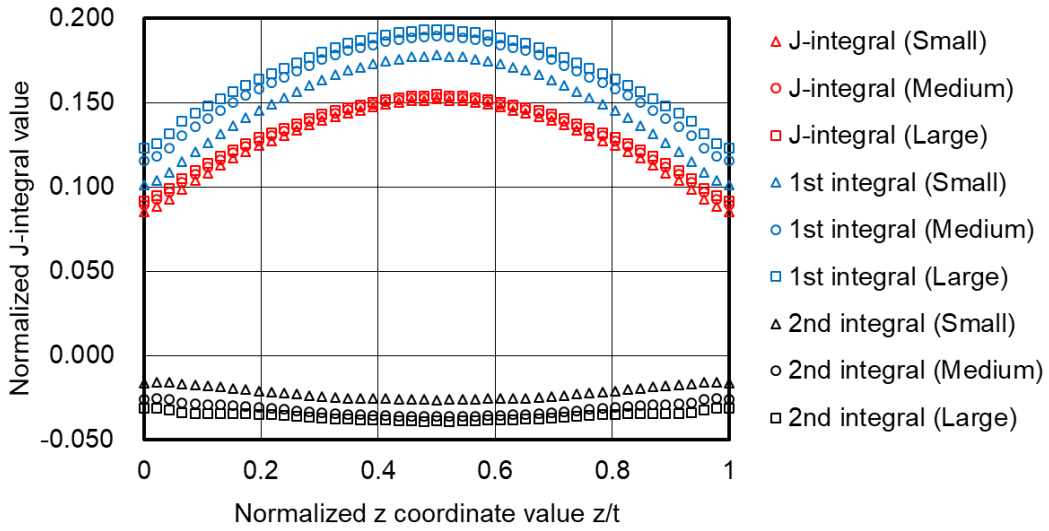

(b) Applied displacement 0.50 mm

Figure 21 Variations of the evaluated J-integral values along the crack front for the problem of the cold work followed by the tensile deformation. [(a) Applied displacement: 0.20 mm, and (b) Applied displacement: 0.50 mm]

3.3 Example problems for a crack in a plate with a homogeneous or non-uniform material undergoing a large elastic-plastic deformation

Some example problems are presented for further demonstration of the path-independent property of the present J-integral formulation. The problems of the CT specimen are considered. The geometries and the finite element discretization are shown in Figures 22 and 23. The finite element model has a total of 232,270 quadratic tetrahedral elements and 322,129 nodes. The length of the element edge along the crack front is 0.25 mm. The finite element analyses were performed by MSC.Marc 2016. It is noted that the thickness of the CT specimen is 1/2 of the ordinary 1TCT geometry.

An isotropic J-2 flow elastic-perfectly plastic constitutive law was assumed. It is noted that the elastic-plastic finite element analyses by MSC.Marc 2016 did not suffer from any serious convergence problems. Three analysis cases are presented in this paper. They assume homogeneous material and decreasing and increasing Young's modulus E and the yield stress σ_Y. The variations of the material properties are expressed by exponential functions as Erdogan [62] assumed. The variations of Young's modulus and the yield

stress when decreasing in the vicinity of the crack front are expressed as

$$E = 1000 \times 10^{-(x-20.48)/10} \text{ (GPa) and } \sigma_Y = 1000 \times 10^{-(x-20.48)/10} \text{ (MPa)} \cdots \quad (28)$$

The variations of Young's modulus and the yield stress when increasing in the vicinity of the crack front are expressed as

$$E = 10 \times 10^{(x-20.48)/10} \text{ (GPa) and } \sigma_Y = 10 \times 10^{(x-20.48)/10} \text{ (MPa)} \cdots\cdots\cdots (29)$$

It is noted that the Young's modulus and the yield stress were set to be 1,000 GPa and 1,000 MPa, respectively, for both the cases in the region of $0 \text{ mm} \le x \le 5.48 \text{ mm}$. Linear variations were assumed between x = 5.48 mm and 20.48 mm, when the values increased in the vicinity of the crack front. Also, the values between x = 40.48 mm and 45.48 mm were assumed to vary linearly when they decreased in the vicinity of the crack front. At the crack front, the Young's modulus and the yield stress were set to be 100 GPa and 100 MPa, respectively, for all cases. The square and circular symbols in Figure 24 show the data points to specify the values of the Young's modulus and the yield stress. The data points were placed every 5 mm. At the data points, the values were assigned by equation (28) or (29) in the vicinity of the crack front (20.48 mm $\le x \le$ 40.8 mm). Then, the values were linearly interpolated between the data points. An analysis with a homogenous material was also performed for a comparison purpose. The values of Young's modulus and the yield stress are shown by the dotted lines. They are 100 GPa and 100 MPa, respectively.

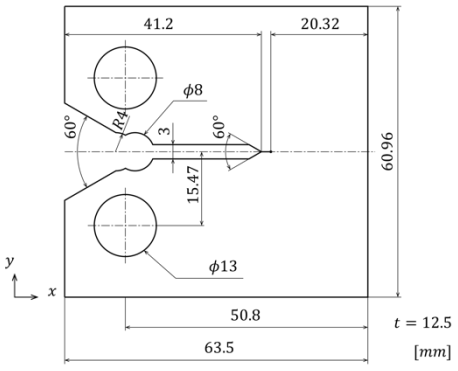

(a) Geometries and the dimensions of the CT specimen

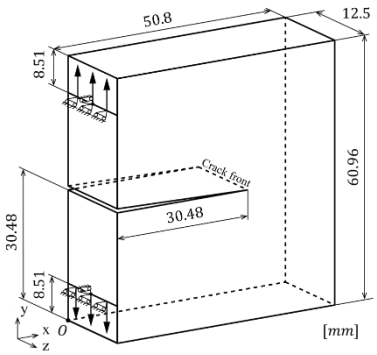

(b) Simplified model of the CT specimen

Figure 22 Geometry of the CT specimen and its simplified model. [(a) Geometries and the dimensions of the CT specimen, and (b) Simplified model of the CT specimen]

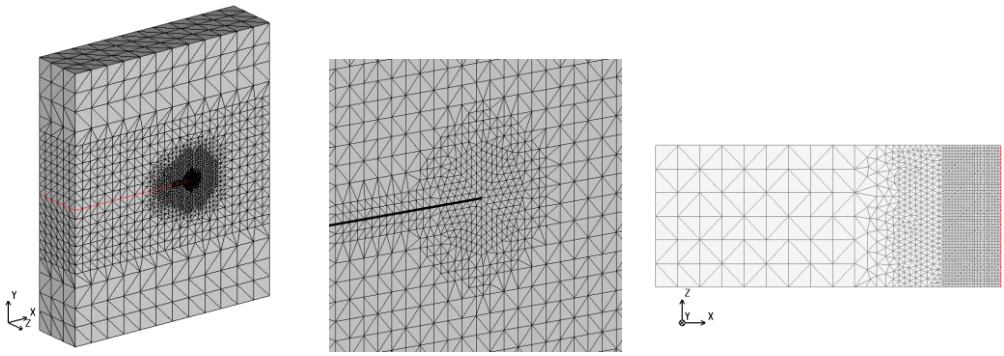

(a) Overall view of the FE model (b) Magnified view of the vicinity of the crack (c) Crack face

Figure 23 Finite element discretization of the simplified CT specimen. [(a) Overall view of the FE model, (b) Magnified view of the vicinity of the crack, and (c) Crack face]

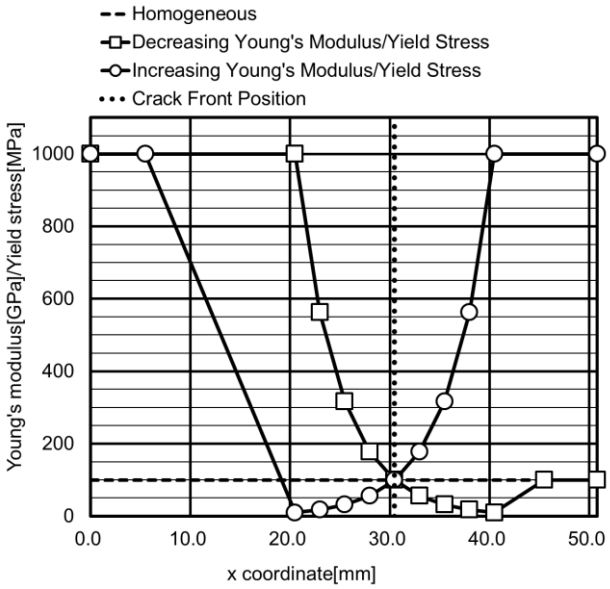

Figure 24 Variations of the Young's modulus and the yield stress.

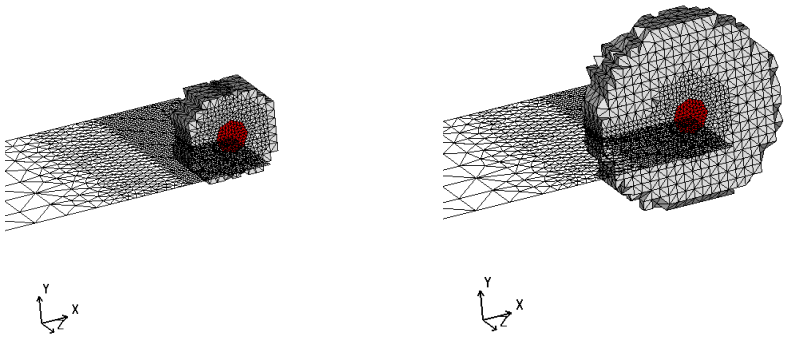

(a) Small (b) Medium

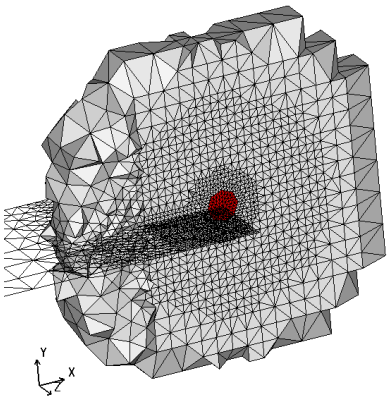

(c) Large

Figure 25 Outer surfaces of small, medium, and large integral domains with ε = 1.0 mm. [(a) Small, (b) Medium, and (c) Large]

The integral domains for the J-integral evaluation were set as follows. The values of Δ and w^o of the assumed integral domain were set to be 10 times the representative size h of the finite element along the crack front. Here, h was 0.25 mm in the present analysis. Therefore, Δ and w^o were 1.25 mm. Three different radii r^o were set. They were 10, 20, and 40 times the element size h. They are designated to be small, medium, and large integral domains in this article. The examples of the actual integral domains are presented in Figure 25. In addition, three different radii ε of the small

volume Ω_ε^o surrounding the crack front are adopted. They are two, three, and four times the size h of elements along the crack front. Therefore, ε was 0.5, 0.75, or 1.0 mm. The small volume Ω_ε^o is also indicated in Figure 25 in red for ε = 1.0 mm.

The results of J-integral evaluations for the homogeneous material case are presented first. The Young's modulus and the yield stress were set to be 100 GPa and 100 MPa, respectively. In Figures 26 and 27, the load-displacement curve and the deformations of the specimen are depicted. The load-displacement curve shows that the specimen experienced highly nonlinear deformation. When the applied displacement reached 3 mm, the crack mouth is seen to open largely. Figures 28 (a)-(d) show the distributions of the evaluated J-integral values along the crack front when the deformations were small and large, respectively. Their load line displacements were 0.03 mm and 3.0 mm. Two different radii ε of the small volume Ω_ε^o surrounding the crack front were adopted. It is observed that when the deformation was small (load-line displacement: 0.03 mm) the evaluated J-integral values with the first integral only were almost the same for two different sizes of integral domains. The magnitudes of the second integrals were very small. The values do not depend on the radius ε of the small volume Ω_ε^o. When the deformation was large (load-line displacement: 3.0 mm), the first integral only depended on the radius of the integral domain, although the material was assumed to be homogeneous. However, the results of the proposed formulation including the second integral are seen to be independent of the size of the integral domain. The radius ε of the small volume Ω_ε^o has some influence on the J-integral value. The J-integral value slightly increased as the radius of ε increased, as seen in the Figures 28 (b) and 28 (d).

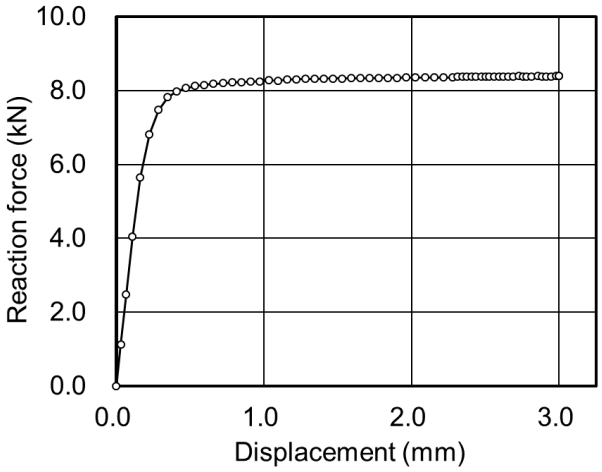

Figure 26 Load-displacement relationship for the case of a homogeneous material.

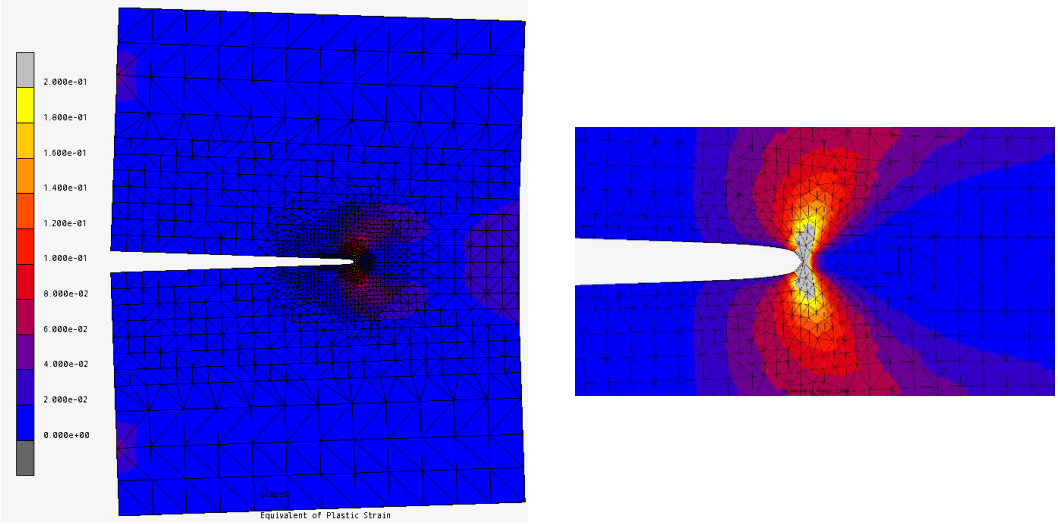

(a) Overall side view (b) Magnified view of the vicinity of the crack front

Figure 27 Deformation and distributions of equivalent plastic strain at a displacement of 3.0 mm. [(a) Overall side view, and (b) Magnified view of the vicinity of the crack front]

.

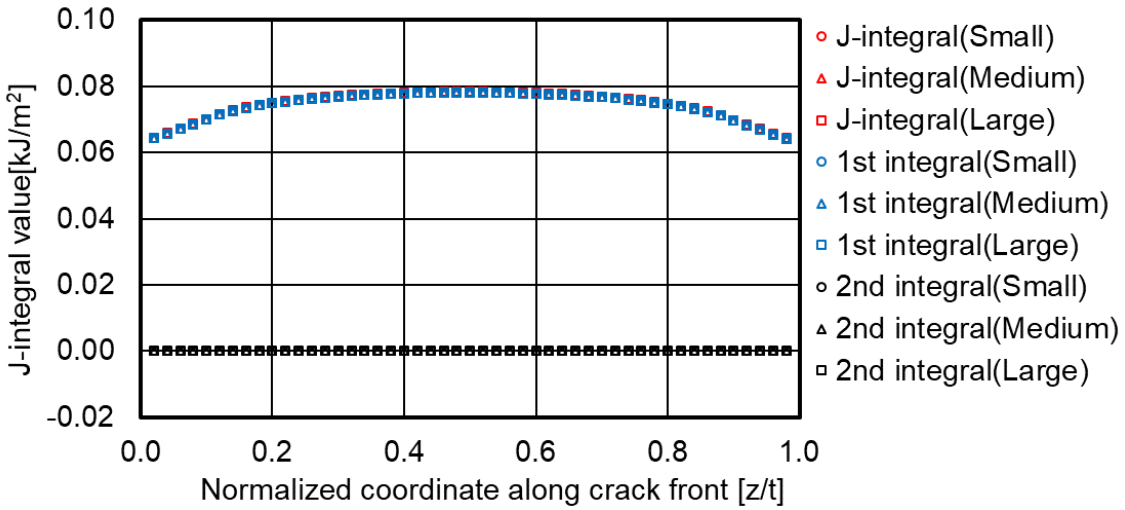

(a) Displacement 0.03 mm and $\varepsilon = 0.5$ mm

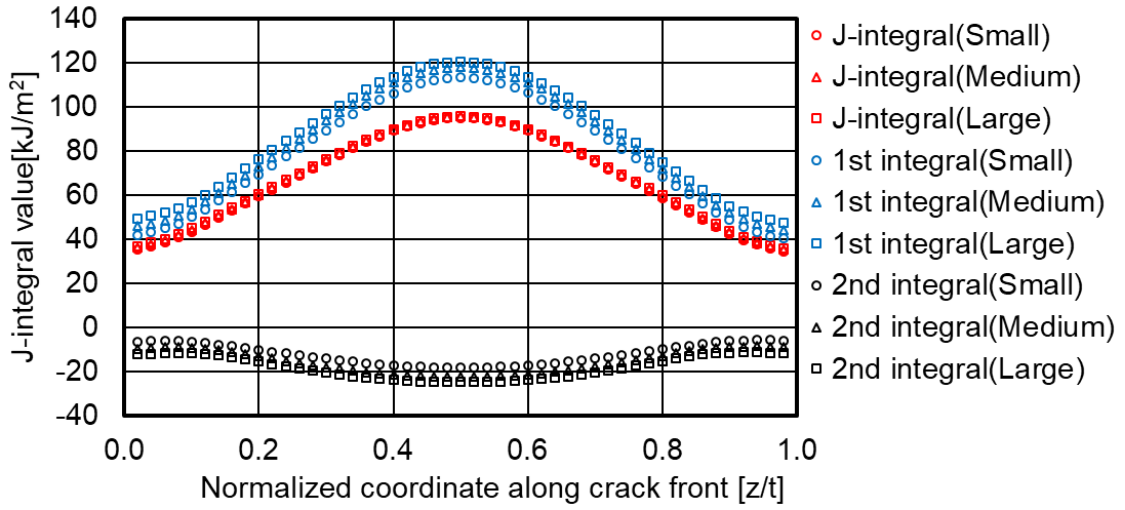

(b) Displacement 3.0 mm and $\varepsilon = 0.5$ mm

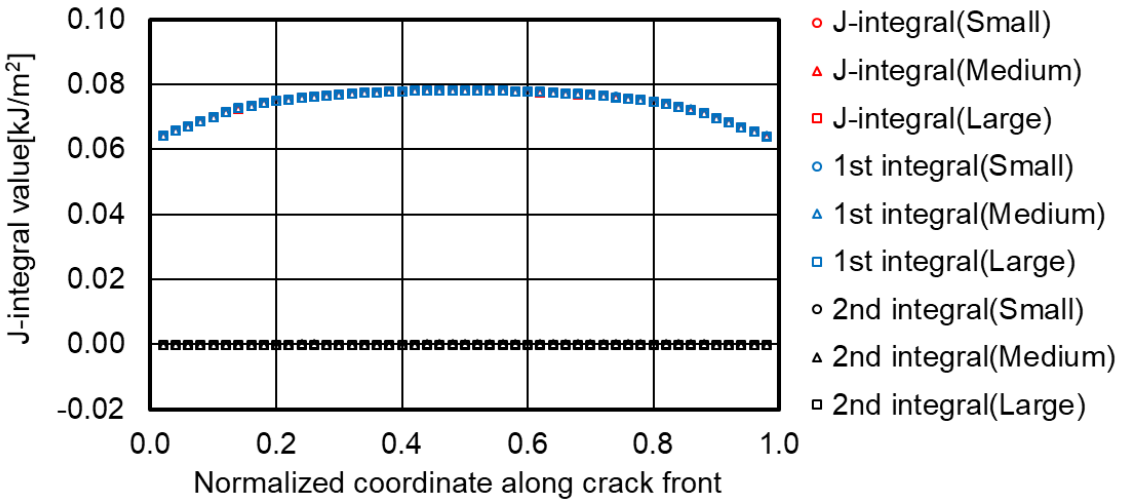

(c) Displacement 0.03 mm and $\varepsilon = 1.0$ mm

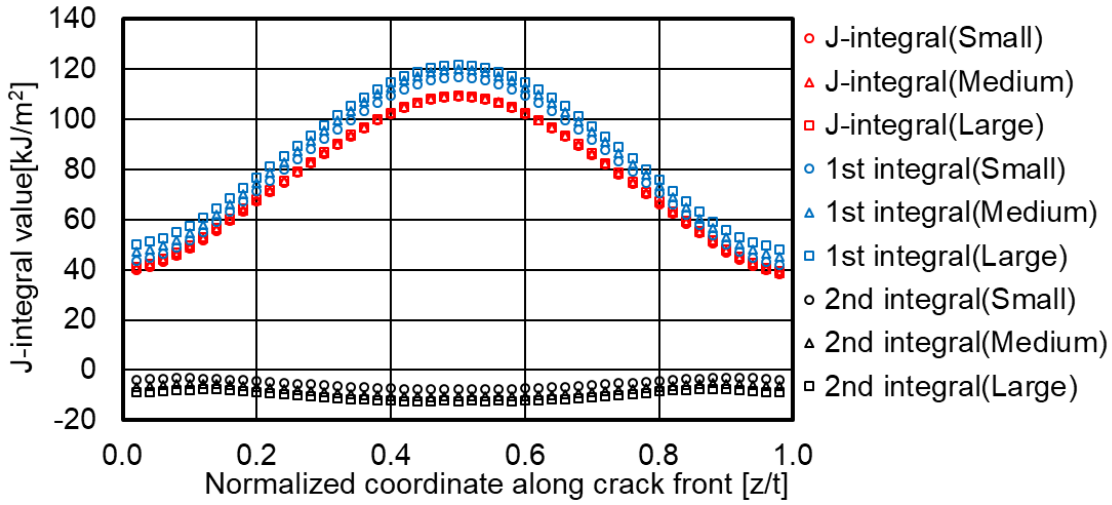

(d) Displacement 3.0 mm and $\varepsilon = 1.0$ mm

Figure 28 Distributions of the evaluated J-integral values along the crack front for various radii ε of near the crack from domain Ω_ε^o and for two magnitudes of the deformations of the CT specimen (0.03 mm and 3.0 mm). [(a) Displacement 0.03 mm and $\varepsilon = 0.5$ mm, (b) Displacement 3.0 mm and $\varepsilon = 0.5$ mm, (c) Displacement 0.03 mm and $\varepsilon = 1.0$ mm, and (d) Displacement 3.0 mm and $\varepsilon = 1.0$ mm]

Some results when the Young's modulus and the yield stress were varied are presented next. As mentioned earlier, Young's modulus and the yield stress were set to vary between

10 GPa and 1,000 GPa as well as 10 MPa and 1,000 MPa, respectively, in the vicinity of the crack front $(20.48\ \text{mm} \le x \le 40.48\ \text{mm})$.

The results of the analyses are presented in Figures 29, 30, and 31. Figure 29 shows the load-displacement relationships. In both cases, the slopes of the curves were almost flat after a certain amount of deformation, indicating that extensive plastic deformations occurred. The distributions of the equivalent plastic strain in both the cases are presented in Figure 30, when the applied displacements were 3.0 mm. Large magnitudes of plastic strains are seen to accumulate in the vicinity of the crack front and at the location of low Young's modulus and yield stress. The distributions of the computed J-integral values are depicted in Figure 31. In Figure 31, the distributions of the J-integral values along the crack front are presented. In Figures 31(a) and 31(b), those when the load line displacement was 0.03 mm are presented. Figures 31(c) and 31(d) show the results when the load line displacement was 3.0 mm. Even when the applied displacement was small (0.03 mm), the results that were computed by the first integral strongly depend on the radius of the integral domain for both cases, as seen in Figures 31(a) and 31(b). However, the J-integral values that were computed by the present formulation are independent of the radius of the integral domain.

Figure 31(c) presents the results of decreasing material constants at the location of the crack front when the applied load-line displacement was large (3.0 mm). The J-integral values computed by the first integral are seen to increase as the size of the integral domain enlarges. When the second integral was included, the evaluated J-integral values recovered the independence with respect to the radius of the integral domain. For the case that the values of the material constants increase, the results of J-integral computations are presented in Figure 31(d). When the large integral domain was adopted, the magnitudes of the first and second integrals were large, but their signs were opposite each other. As a result, the magnitude of the J-integral value was much smaller than the first or second integral alone. The magnitudes of the first and second integrals that were evaluated with the small and medium integral domains were much smaller than those computed with the large integral domain. The J-integral values for the totals of the first and second integrals are similar in the sense that they are both small. Therefore, the path-independent property seems to hold in this example problem compared with the magnitudes of the first or second integrals when computed with the large integral domain.

From the numerical results presented in this section, it can be concluded that the proposed J-integral formulation can guarantee the path-independent property, even if the mechanical properties of the material have steep spatial variations in the vicinity of the crack front. The mechanical properties include the elastic moduli as well as those for the nonlinear deformation, such as the yield stress.

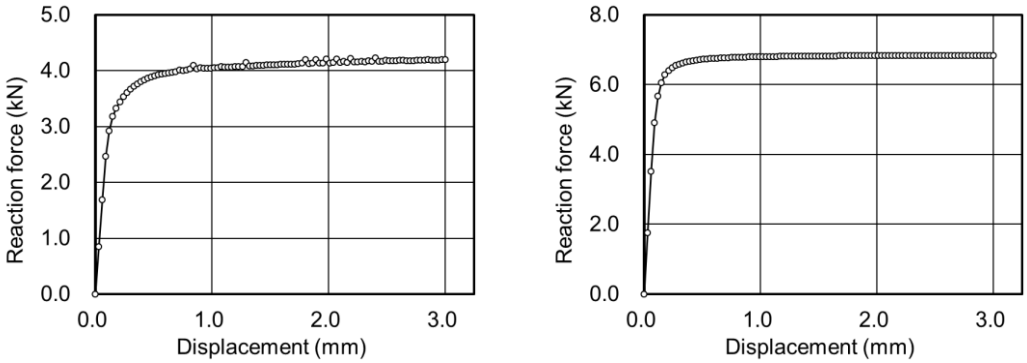

(a) Decreasing yield stress and Young's modulus.

(b) Increasing yield stress and Young's modulus

Figure 29 Load-displacement curves. [(a) Decreasing yield stress and Young's modulus, and (b) Increasing yield stress and Young's modulus]

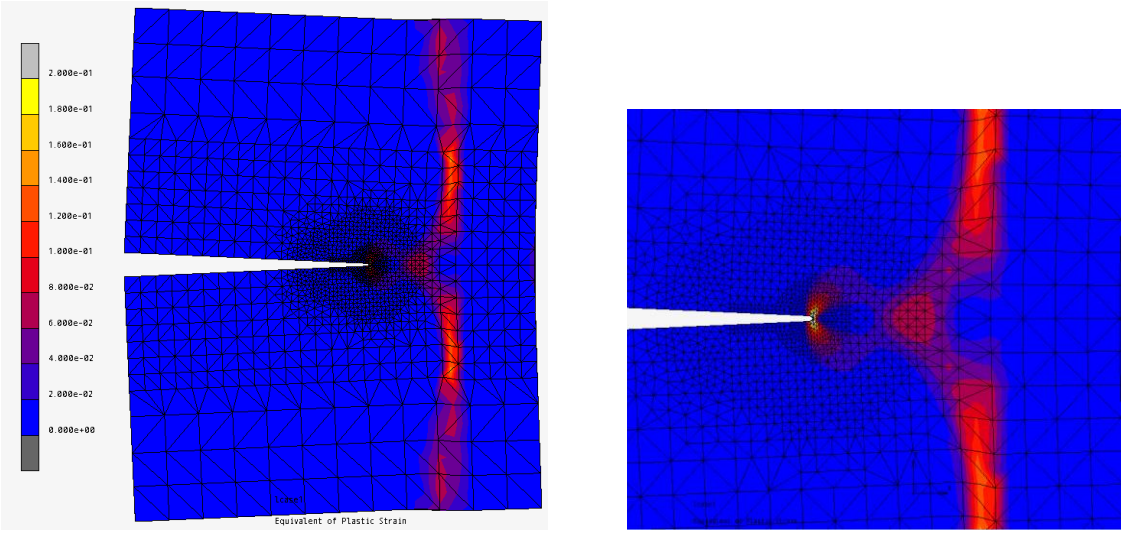

(a) Case of decreasing yield stress and Young's modulus in the vicinity of the crack front (left: overall view, and right: vicinity of the crack front)

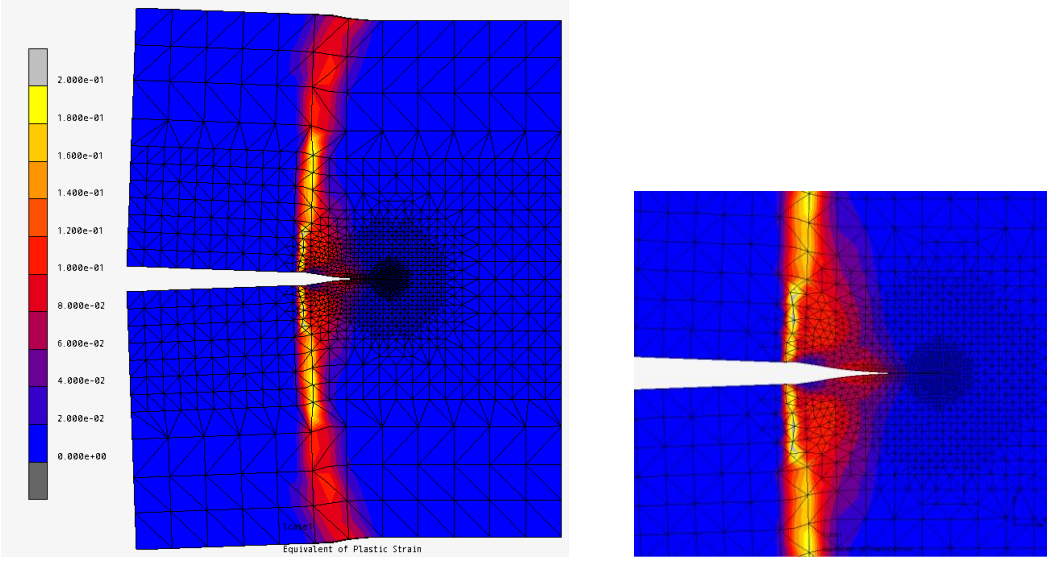

(b) Case of increasing yield stress and Young's modulus in the vicinity of the crack front (left: overall view, and right: vicinity of the crack front)

Figure 30 Deformations and the distributions of the equivalent plastic strain for the cases of decreasing and increasing yield stress and Young's modulus in the vicinity of the crack front. [(a) Case of decreasing yield stress and Young's modulus in the vicinity of the crack front (left: overall view, and right: vicinity of the crack front), and (b) Case of increasing yield stress and Young's modulus in the vicinity of the crack front (left: overall view, and right: vicinity of the crack front)]

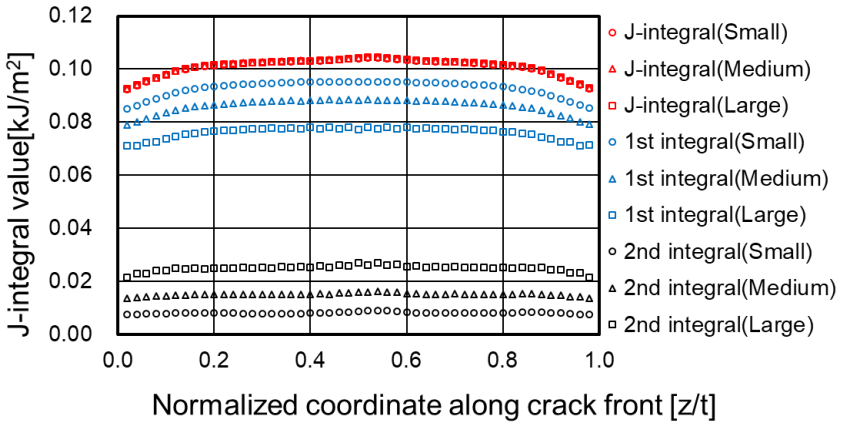

(a) Decreasing yield stress and Young's modulus; load line displacement: 0.03 mm

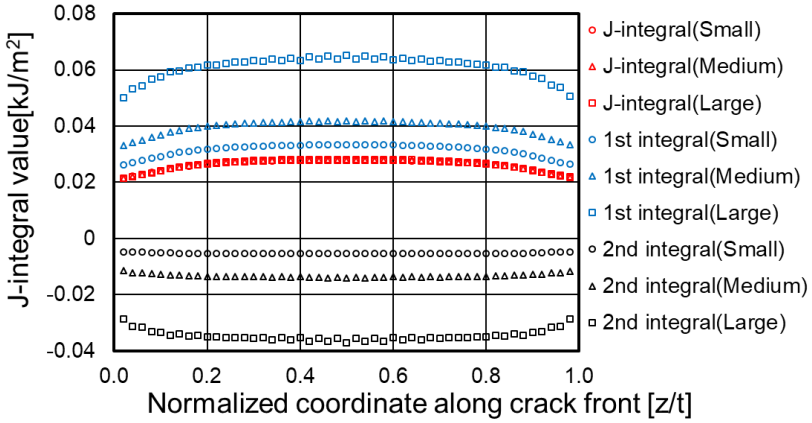

(b) Increasing yield stress and Young's modulus; load line displacement: 0.03 mm

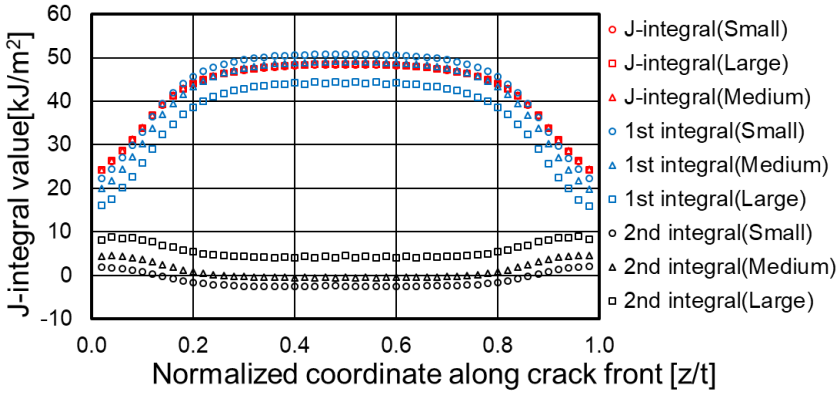

(c) Decreasing yield stress and Young's modulus; load line displacement: 3.00 mm

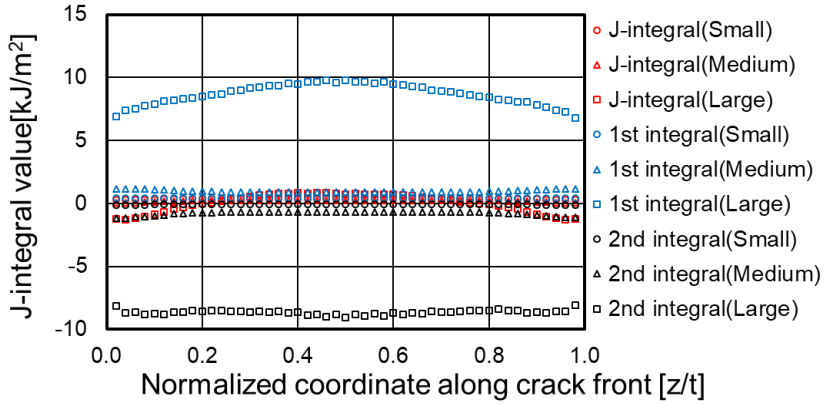

(d) Increasing yield stress and Young's modulus; load line displacement: 3.00 mm

Figure 31 Distributions of the evaluated J-integral values along the crack front. [(a) Decreasing yield stress and Young's modulus; load line displacement: 0.03 mm, (b) Increasing yield stress and Young's modulus; load line displacement: 0.03 mm, (c) Decreasing yield stress and Young's modulus; load line displacement: 3.00 mm, and (d) Increasing yield stress and Young's modulus; load line displacement: 3.00 mm]

4. Discussions

In the previous publication of Nose et al. [11], a linear fracture mechanics analysis methodology under weld residual stresses was presented. The stress intensity factors were evaluated by the virtual crack closure-integral method (VCCM) [12], which was valid only for linear elastic materials. It could include the effects of the weld residual stresses as initial stresses. It does not require any deformation-history-dependent parameters. In the present paper, a method to compute the J-integral under the influences of residual stresses is presented. Residual stresses are generally produced by processes such as plastic work and welding. The computation of the strain energy generally requires complete deformation histories. On the other hand, it is sometimes difficult to know the complete deformation history. Residual stresses are sometimes measured by experiment or estimated by empirical formula. In such cases, complete deformation histories are not known. The present paper describes such scenarios. In the numerical examples dealing with the problems of plate bending and cold work of a hole, only the residual stresses were transferred to the fracture mechanics analyses assuming the cracks. The results of the present J-integral evaluations showed the path-independent property. Hence, the proposed J-integral formulation of equation (26) is considered to be valid even when the complete deformation history is not known. However, it should be noted that the present formulation cannot deal with material property changes due to the deformation histories. In other words, without the information of complete deformation history, parameters including the yield stress and back stresses cannot be set because they depend on the prior deformation histories. In the present investigation, numerical examples were designed such that the influences of the changes of these parameters were very small. It was accomplished by assuming a very low hardening modulus. Therefore, the strain hardening could be assumed to be small and so was neglected. The issue of the material property change due to the prior-deformation history remains.

When the deformations were very small, the influences of the residual stresses were so significant that the first integral of equation (26) strongly depended on the size of integral domain. The contribution of the second integral recovered the path-independent property. It was also found that the influences of the residual stresses weakened as the deformation progressed. The contribution of the second integral was found to decrease. It is, however, noted that the second integral was necessary to keep the path-independent property for

large strain elastic-plastic problems.

In the example problems of the nonuniform mechanical properties of the material, the proposed J-integral was found to be path-independent for almost all cases. It was clear that the results of the first integral alone did not possess the path-independent property. The inclusion of the second integral recovered the path-independent property. It was a natural consequence of the way the present formulation was derived. No assumption was made on the material properties except that the material properties did not have any discontinuous spatial changes. Therefore, the present formulation is applicable to the cases of spatially changing material behavior, such as the functionally graded materials.

The proposed three-dimensional J-integral formulation can deal with large deformation elastic-plastic fracture problems with residual stresses and with spatially changing mechanical properties of the material. Furthermore, we did not pose any assumptions on the constitutive model in the derivation. Therefore, the proposed three-dimensional J-integral is applicable to any nonlinear fracture mechanics problem. On the other hand, the proposed J-integral expresses the deformation energy dissipating into the cylindrical shaped volume of radius ε and length unity. We may consider ε to be the representative radius of the process zone. Therefore, the evaluated J-integral value depends on the radius ε. Hence, we may regard the proposed three-dimensional J-integral as expressing the deformation energy dissipating into the process zone per unit crack extension. This feature is the same as the T_ε^* integral for two-dimensional problems. Hence, we may name the present J-integral to be T_ε^{*3D} which is the three-dimensional version of T_ε^*.

Although the J-integral formulation that has a mean of energy dissipation into the process zone and holds the path-independent property regardless of the magnitude of deformation and material property gradients, it has been known that the J-integral alone could not completely characterize the near-tip deformation field. Yang et al. [63] presented a higher order asymptotic crack tip solution for a power-law hardening material, leading to the establishment of the J-A theory. J-A theory is a two-parameter fracture mechanics model in which J-integral and A characterize the HRR field (see Hutchinson [64] and Rice and Rosengren [65]) and the higher order asymptotic solution, respectively. Nikishikov et al.

[66] demonstrated that the two-parameter J-A approach could characterize the near-crack tip stress distributions under various crack configurations, such as edge crack tension, center crack tension, three-point bend and compact tension specimens. The two-parameter J-A approach was applied to the three-dimensional crack problems by Matvienko et al. [67]. It became clear through the series of investigations on the two-parameter J-A approach, the J-integral alone could not fully characterize the crack tip deformation field. Although the present J-integral as T_{ε}^{*3D} has a mean of energy dissipation into the process zone, it cannot fully characterize the singular deformation field in the vicinity of the crack front. Further investigations are needed to clarify the asymptotic fields in the vicinity of the crack front when the material undergoes a large deformation and has some spatial changes in its mechanical properties.

5. Conclusions

In this paper, a general formulation of the J-integral for solids with inhomogeneous materials and solids with some prior deformation histories is presented in a unified manner. We summarize the outcomes of the present investigation, as follows:

- The proposed J-integral formulation can be applied to large deformation elastic-plastic problems with spatially varying mechanical properties of a material.
- The proposed J-integral formulation can be applied to problems with residual stresses. The complete deformation histories need not be known, even though the strain energy density is involved in the J-integral formulation.
- The proposed J-integral formulation expresses energy dissipation into a cylindrical volume of radius ε and length unity. The value depends on the radius ε of the cylinder.
- The proposed J-integral can be regarded as the deformation energy dissipating into the process zone, the size of which is characterized by radius ε.
- Finally, the proposed J-integral can be considered to be a rigorous extension of the two-dimensional T_{ε}^{*} integral of Okada and Atluri [41]. We may name it to be T_{ε}^{*3D} as the three-dimensional version of T_{ε}^{*}. Therefore, by considering the moving and

elongating process zone model as discussed in [41], the proposed T_{ε}^{*3D} is expected give further insights into three-dimensional elastic-plastic crack propagation phenomena.

Acknowledgements

Precious and fruitful discussions with Mr. K. Chiba of Nissan Motor Co., Ltd., Professors H. Murakawa and H. Serizawa of the Joining and Welding Research Institute of Osaka University, Professors M. Shibahara and K. Ikushima of Osaka Prefecture University, and Dr. A. Kawahara of Osaka Prefecture University are gratefully acknowledged. Part of the present research was performed under a Grant-in-Aid for Scientific Research (16K05988) "Nonlinear fracture mechanics analyses considering the material nonuniformities in and the vicinities of welded joints" from the Japan Society for the Promotion of Science. The support is gratefully acknowledged.

References

[1] Ueda Y, Ronda J, Murakawa H, Ikeuchi K. Thermo-Mechanical-Metallurgical Model of Welded Steel Part I: Evolutions for Internal Material Structures. Trans. JWRI 1994; 23 (2): 149-167.

[2] Ronda J, Murakawa H, Oliver G, Ueda Y. Thermo-Mechanical-Metallurgical Model of Welded Steel Part II: Finite Element Formulation and Constitutive Equations. Trans. JWRI 1995; 24 (2): 93-113.

[3] Maekawa A, Serizawa H, Murakawa H. Fast Computation Based on an Iterative Substructure on an Iterative Substructure Method for Three-Dimensional Simulation of Multipass Welding. Journal of Pressure Vessel Technology 2015; 137; 041410-1, DOI: 10.1115/1.4031376.

[4] Maekawa A, Kawahara A, Serizawa H, Murakawa H. Prediction of Weld Residual Stress in a Pressurized Water Reactor Pressurizer Surge Nozzle. Journal of Pressure Vessel Technology 2016; 138; 02140-1, DOI:10.1115/1.4031376.

[5] Broussard III JE, Standardized Through-Wall Distributions of Dissimilar Metal Weld Residual Stress, ASME 2015 Pressure Vessels and Piping Division Conference PVP 2015, 2015 in Boston, Massachusetts, USA, PVP2015-45950.

[6] Chakherlou TN, Vogwell JT. A Novel Method of Cold Expansion which Creates Near-Uniform Compressive Tangential Residual Stress Around a Fastener Hole. Fatigue and Fracture of Engineering Materials & Structures 2004; 27 (5): 343-351.

[7] Pavier MJ, Poussard CGC, Smith DJ. Effect of Residual Stress Around Cold Worked Holes on Fracture under Superimposed Mechanical Load. Engineering Fracture Mechanics 1999; 63: 751-773.

[8] Marannano G, Virz` Mariotti G, D'Acquisto L, Restivo G, Gianaris N. Effect of Cold Working and Ring Indentation on Fatigue Life of Aluminum Alloy Specimens. Experimental Techniques 2015; 39: 19-27, DOI:10.1111/ext.12018.

[9] Rasty J, Chapman D. Isothermal and Thermomechanical Finite-Element Analysis of the Tube Drawing Process Using a Fixed Tapered Plug. Journal of Materials Engineering and Performance 1992; 1 (4): 547-554.

[10] Yang YY, Zhao LH, Sun ZZ. Study on Mechanism of Cylindrical Shallow Shell Surface Deflection. Journal of Materials Processing Technology 2007; 187-188: 145-149, DOI:10.1016/j.jmatprotec.2006.11.176.

[11] Nose N, Amano H, Okada H, Yusa Y, Maekawa A, Kamaya M, Kawai H. Computational Crack Propagation Analysis with Consideration of Weld Residual Stresses, Engineering Fracture Mechanics 2017; 182, pp: 708-731. DOI: http://dx.doi.org/10.1016/j.engfracmech.2017.06.022

[12] Okada, H, Kawai, H, Araki, K. A Virtual Crack Closure-Integral Method (VCCM) to Compute the Energy Release Rates and Stress Intensity Factors based on Quadratic Tetrahedral Finite Elements. Engineering Fracture Mechanics 2008; 75: 4466–4485, DOI: 10.1016/j.engfracmech.2008.04.014.

[13] Yonezu A, Akimoto H, Fujisawa S, Chen X. Spherical Indentation Method for Measuring Local Mechanical Properties of Welded Stainless Steel at High Temperature. Materials and Design 2013; 52: 812-820, DOI: 10.1016/j.matdes.2013.06.015.

[14] Kim JJ, Pham T-H, Kim S-E. Instrumented indentation testing and FE analysis for investigation of mechanical properties in structural steel weld zone. International Journal of Mechanical Sciences 2915; 103: 265-274, DOI: 10.1016/j.ijmecsci.2015.09.015.

[15] Niino M, Maeda S. Recent Development Status of Functionally Gradient Materials. ISIJ International 1990; 30 (9): 699-703.

[16] Koizumi M. FGM Activities in Japan. Composites Part B 1997; 28B: 1-4.

[17] Watanabe Y, Sato H, Fukui Y. Wear Properties of Intermetallic Compound Reinforced Functionally Graded Materials Fabricated by Centrifugal Solid-Particle and In-Situ Methods. Journal of Solid Mechanics and Materials Engineering 2008; 2 (7): 842-853, DOI: 10.1299/jmmp.2.842.

[18] Zuback JS, Palmer TA, DebRoy T. Additive Manufacturing of Functionally Graded Transition Joints between Ferritic and Austenitic Alloys. Journal of Alloys and Compounds 2018; 770: 995-1003, DOI: 10.1016/j.jallcom.2018.08.197.

[19] Hojo, K, Kawabata S. Mode I Ductile Crack Growth of CT Specimen under large Cyclic Loading. ASME 2017 Pressure Vessels and Piping Division Conference PVP 2017, 2017 in Waikoloa, Hawaii, USA, PVP2017-65691.

[20] Hojo K, Kawabata S, Ogawa N. Mode I Ductile Crack Growth of 1TCT Specimen Under Large Cyclic Loading (Part II). ASME 2018 Pressure Vessels and Piping Division Conference PVP 2018, 2018 in Prague, Czech Republic, PVP2018-84383.

[21] Hojo K. Mode I Ductile Crack Growth of 1TCT Specimen Under Large Cyclic Loading: Part III. ASME 2019 Pressure Vessels and Piping Division Conference PVP 2019, 2019 in San Antonio, Texas, USA, PVP2019-93476.

[22] Boyce BL, Kramer SLB, Fang HE, Cordova TE, Neilsen MK, Dion K, Kaczmarowski AK, Karasz E, Xue L, Gross AJ, Ghahremaninezhad A, Ravi-Chandar K, Lin S-P., Chi S-W, Chen JS, Yreux E, Rüter M, Qian Q, Zhou Z, Bhamare S, O'Connor DT, Tang S, Elkhodary KI, Zhao J, Hochhalter JD, Cerrone AR, Ingraffea AR, Wawrzynek PA, Carter BJ, Emery JM, Veilleux MG, Yang P,

Gan Y, Zhang X, Chen Z, Madenci E, Kilic B, Zhang T, Fang E, Liu P, Lua J, Nahshon K, Miraglia M, Cruce J, DeFrese R, Moyer ET, Brinckmann S, Quinkert L, Pack K, Luo M, Wierzbicki T. The Sandia Fracture Challenge: Blind Round Robin Predictions of Ductile Tearing. International Journal of Fracture 2014; 165: 5-68, DOI:10.1007/s10704-013-9904-6.

[23] Boyce BL, Kramer SLB, Bosiljevac TR, Corona E, Moore JA, Elkhodary K, Simha CHM, Williams BW, Cerrone AR, Nonn A, Hochhalter JD, Bomarito GF, Warner JE, Carter BJ, Warner DH, Ingraffea AR, Zhang T, Fang X, Lua J, Chiaruttini V, Mazière M, Feld-Payet S, Yastrebov VA, Besson J, Chaboche J-L, Lian J, Di Y, Wu B, Novokshanov D, Vajragupta N, Kucharczyk P, Brinnel V, Döbereiner B, Münstermann S, Neilsen MK, Dion K, Karlson KN, Foulk III JW, Brown AA, Veilleux MG, Bignell JL, Sanborn SE, Jones CA, Mattie PD, Pack K, Wierzbicki T, Chi S-W, Lin S-P, Mahdavi A, Predan J, Zadravec J, Gross AJ, Ravi-Chandar K, Xue L. The Second Sandia Fracture Challenge: Predictions of Ductile Failure under Quasi-Static and Moderate-Rate Dynamic Loading. International Journal of Fracture 2016; 198: 5-100, DOI: 10.1007/s10704-016-0089-7.

[24] Kramer SLB, Jones A, Mostafa A, Ravaji B, Tancogne-Dejean T, Roth CC, Bandpay MG, Pack K, Foster JT, Behzadinasab M, Sobotka JC, McFarland JM, Stein J, Spear AD, Newell P, Czabaj MW, Williams B, Simha H, Gesing M, Gilkey LN, Jones CA, Dingreville R, Sanborn SE, Bignell JL, Cerrone AR, Keim V, Aida Nonn A, Cooreman S, Thibaux P, Ames N, Connor DO, Parno M, Davis B, Tucker J, Coudrillier B, Karlson KN, Ostien JT, Foulk III JW, Hammetter CI, Grange S, Emery JM, Brown JA, Bishop JE, Johnson KL, Ford KR, Brinckmann S, Neilsen MK, Jackiewicz J, Ravi-Chandar K, Ivanoff T, Salzbrenner BC, Boyce BL. The Third Sandia Fracture Challenge: Predictions of Ductile Fracture in Additively Manufactured Metal. International Journal of Fracture 2019; 218: 5-61, DOI: 10.1007/s10704-019-00361-1.

[25] Rice JR. A Path Independent Integral and the Approximate Analysis of Strain Concentration by Notches and Cracks. Journal of Applied Mechanics 1968; 35: 379-386.

[26] Eshelby DJ. The Continuum Theory of Lattice Defects. Solid State Physics 1956: 3; 79-144.

[27] Cherepanov GP. Crack propagation in continuous media. Journal of Applied Mathematics and Mechanics 1967: 31 (3); 503-512, DOI: 10.1016/0021-8928(67)90034-2.

[28] Blackburn WS. Path independent integrals to predict onset of crack instability in an elastic plastic material. International Journal of Fracture 1972: 8; 343-346, DOI: 10.1007/BF00186134.

[29] Amestoy M, Bui H D, Labbens R. On the definition of local path independent integrals in three-dimensional crack problems. Mechanics Research Communications 1981: 8 (4); 231-236, DOI: 10.1016/0093-6413(81)90058-6.

[30] Kubo S, Ohji K. A theoretical study on J-integrals of three-dimensional cracks. Journal of the Society of Materials Science, Japan q981: 30 (335); 796-802, DOI: 10.2472/jsms.30.796

[31] Kikuchi M, Miyamoto H, Ishida K. Three-Dimensional J Integral: 1st Report, J Integral of Through Cracks and Surface Cracks in Elastic Body). The Japan Society of Mechanical Engineers Series A 1983; 49 (439): 314-321.

[32] Kikuchi M, Miyamoto H, Tanaka M. J integral evaluation of CT specimen in elastic-plastic state. Bulletin of JSME (Japan Society of Mechanical Engineers) 1984; 27 (233): 2365-2371.

[33] Ando Y, Yagawa G, Ishihara K. Three-dimensional non-linear fracture analysis related to thermal shock. Transactions of the Japan Society of Mechanical Engineers Series A 1983: 49 (439) ; 304-313, DOI: 10.1299/kikaia.49.304.

[34] Li FZ, Shih CF, Needleman A. A Comparison of Methods for Calculating Energy Release Rates. Engineering Fracture Mechanics 1985; 21 (2): 405-421.

[35] deLorenzi HG. On the Energy Release Rate and the J-Integral for 3-D Crack Configurations. International Journal of Fracture 1982; 19: 183-193.

[36] Nikishkov GP, Atluri SN. An Equivalent Domain Integral Method for Computing Crack-Tip Integral Parameters in Non-Elastic, Thermo-Mechanical Fracture. Engineering Fracture Mechanics 1987; 26: 851-867.

[37] Nikishkov GP, Atluri SN. Three-Dimensional Elastic-Plastic J-Integral Calculations for Semielliptical Surface Cracks in a Tensile Plate. Engineering Fracture Mechanics 1988; 29: 81-87.

[38] Atluri SN, Nishioka T, Nakagaki M. Incremental path-independent integrals in inelastic and dynamic fracture mechanics. Engineering Fracture Mechanics 1984; 20 (2): 209-244.

[39] Brust FW, Nishioka T, Atluri SN, Nakagaki M. Further Studies on Elastic-Plastic Stable Fracture Utilizing the T* Integral. Engineering Fracture Mechanics 1985; 22 (6): 1079-1103.

[40] Brust FW, Nakagaki M, Springfield C. Integral Parameters for Thermal Fracture. Engineering Fracture Mechanics 1989; 33 (4): 561-579.

[41] Okada H, Atluri SN. Further studies on the characteristics of the T_ε^* integral: Plane stress stable crack growth in ductile materials. Computational Mechanics 1999; 23; 339-352.

[42] Omori Y, Kobayashi AS, Okada H, Atluri SN, Tan, PW. T_ε^* Integral as a Crack Growth Criterion. Mechanics of Materials 1998; 28: 147-154.

[43] Okada H, Atluri SN, Omori Y, Kobayashi AS. Direct Evaluation of T_ε^* Integral from Experimentally Measured Near Tip Displacement Field, for a Plate with Stably Propagating Crack. International Journal of Plasticity 1999; 15: 869-897.

[44] Carka D, Landis CM. On the Path-Dependence of the J-Integral Near a Stationary Crack in an Elastic-Plastic Material. Journal of Applied Mechanics 2011; 78: 011006; 1-6, DOI: 10.1115/1.4001748.

[45] Carka D, Landis CM, McMeeking RM. A Note on the Path-Dependence of the J-Integral Near a Stationary Crack in an Elastic-Plastic Material With Finite Deformation. Journal of Applied Mechanics 2012; 79(4): 044502, DOI:10.1115/1.4006255.

[46] Koshima T, Okada H. Three-Dimensional J-Integral Evaluation for Finite Strain Elastic-Plastic Solid using the Quadratic Tetrahedral Finite Element and Automatic Meshing Methodology, Engineering Fracture Mechanics 2015; 135: 34-63, DOI:10.1016/j.engfracmech.2015.01.014.

[47] Zienkiewicz, OC, Zhu, JZ. The Superconvergent Patch Recovery (SPR) and Adaptive Finite Element Refinement. Computer Methods in Applied Mechanics and Engineering 1992; 101: 207-224.

[48] Zienkiewicz, OC, Zhu, JZ. Superconvergence and the Superconvergent Patch Recovery. Finite Elements in Analysis and Design 1995; 19: 11-23.

[49] Arai K, Okada H, Yusa Y. Formulation of Three-Dimensional J-Integral for Finite Strain Elastic-Plastic Fracture Problems under any Load Histories (Monotonic and Cyclic Loads). ASME 2018 Pressure Vessels and Piping Division Conference PVP 2018, 2018 in Prague, Czech Republic, PVP2018-84241.

[50] Arai K, Okada H, Yusa Y. A New Three-Dimensional J-Integral Formulation for Arbitrary Load History and Finite Deformation. Transactions of the JSME (in Japanese) 2018; 84 (863): 18-00115, DOI:10.1299/transjsme.18-00115.

[51] Arai K, Okada H, Yusa Y. A New Formulation of J-Integral Range ΔJ using Three-Dimensional Equivalent Domain Integral for Finite Deformation Elastic-Elastic

Problem. Transactions of the JSME (in Japanese) 2018; 84 (867): 18-00309, DOI: 10.1299/transjsme.18-00309.

[52] Yildirim B. An Equivalent Domain Integral Method for Fracture Analysis of Functionally Graded Materials under Thermal Stresses. Journal of Thermal Stresses 2006; 29: 371-397. DOI: 10.1080/01495730500499175

[53] Moghaddam AS. Alfano M. Determination of Stress Intensity Factors of 3D Curved Non-Planer Cracks in FGMs Subjected to Thermal Loading. Engineering Fracture Mechanics 2015; 146: 172-184. DOI: 10.1016/j.engfracmech.2015.07.040

[54] Hein J, Kuna M. 3D J-Integral for Functionally Graded and Temperature Dependent Thermoelastic Materials. Procedia Structural Integrity 2016; 2: 2462-2254. DOI: 10.1016/j.prostr.2016.06.281.

[55] Park JS, Choi YH, Kim J, Seyoung Im S. Energy Release Rate in the Presence of Residual and Thermal Stresses. International Journal of Solids and Structures 2015; 59: 73-78, DOI:10.1016/j.ijsolstr.2015.01.013.

[56] Jin ZH, Dodds Jr. RH. Crack Growth Resistance Behavior of a Functionally Graded Material: Computational Studies. Engineering Fracture Mechanics 2004; 71: 1651-1672.

[57] Wang Z, Nakamura T. Simulations of Crack Propagation in Elastic-Plastic Graded Materials. Mechanics of Materials 2004; 36: 601-622. DOI: 10.1016/S0167-6636(03)00079-6.

[58] Okada H, Kadowaki S, Suzuki M, Yusa Y. J-Integral Computation for Elastic-Plastic Materials with Spatially Varying Mechanical Properties. Engineering Fracture Mechanics 2019; 207: 181-202, DOI: 10.1016/j.engfracmech.2018.12.029.

[59] Atluri SN. Energetic approaches and path-independent integrals in fracture mechanics, Computational Methods in Mechanics of Fracture, Ed by Atluri, S.N., 1986, 121-165.

[60] Okada H, Ohata S. Three-Dimensional J-Integral Evaluation for Cracks with Arbitrary Curvatures and Kinks based on Domain Integral Method for Quadratic Tetrahedral Finite Element. Engineering Fracture Mechanics 2013; 109: 58-77, DOI: 10.1016/j.engfracmech.2013.06.009.

[61] MSC Software Corporation, Marc® 2016 Volume A: Theory and User Information. 2016.

[62] Erdogan F. Fracture Mechanics of Functionally Graded Materials. Composites Engineering 1995; 5 (7): 753-770.

[63] Yang S, Chao YJ, Sutton MA., Higher-order asymptotic fields in a power law hardening material. Engineering Fracture Mechanics 1993: 45; 1-20, DOI: 10.1016/0013-7944(93)90002-A.

[64] Hutchinson JW. Plastic stress and strain fields at a crack tip. Journal of the Mechanics and Physics of Solids 1968: 16 (5); 337-342, DOI: 10.1016/0022-5096(68)90021-5.

[65] Rice JR, Rosengren GF. Plane strain deformation near a crack tip in a power-law hardening material. Journal of Mechanics and Physics of Solids 1968: 16 (1); 1-12, DOI: 10.1016/0022-5096(68)90013-6.

[66] Nikishkov GP, Bruckner-Foit A, Munz D. Calculation of the second fracture parameter for finite cracked bodies using a three-term elastic-plastic asymptotic expansion. Engineering Fracture Mechanics 1995: 52; 685-701, DOI: 10.1016/0013-7944(95)00024-P.

[67] Matvienko YG, Nikishkov GP. Two-parameter J-A concept in connection with crack-tip constraint. Theoretical and Applied Fracture Mechanics 2017: 92; 306-317, DOI: 10.1016/j.tafmec.2017.04.007.

List of figures

spring back. [(a) Equivalent plastic strain, and (b) Stress σ_{zz}]

Figure 10 Comparison between the distributions of the residual stress S_{zz} in the x-direction at the center of the plate, that computed under the assumption of the Euler-Bernoulli beam theory, and that evaluated by the present finite element analysis.

Figure 11 Load-displacement curve when the plate was subject to a tensile load.

Figure 12 Distribution of equivalent plastic strain at U_z = 0.15 mm.

Figure 13 Examples of integral domains having radii r^o of the integral domain $\Omega^o_{Int.}$ of (a) 0.30 mm, (b) 0.54 mm, and (c) 0.75 mm. They are designated to be small, medium, and large integral domains, respectively. [(a) r^o = 0.30 mm (small), (b) r^o = 0.54 mm (medium), and (c) r^o = 0.75 mm (large)].

Figure 14 Distributions of the evaluated J-integral values by the present formulation [(a) Applied displacement 0.02 mm and (b) Applied displacement 0.150 mm].

Figure 15 Schematic diagram of the problem of cold working of a circular hole in a flat plate. Then, a through crack is assumed at the edge of the hole, and the plate is subject to a tensile load. [(a) Geometries of the plate, the hole, and the crack, (b) Problem of cold work, and (c) Plate with a circular hole subject to a tensile load]

Figure 16 Finite element model for the problem of cold work, followed by tensile deformation.

Figure 17 Variations of the residual stresses with respect to the distance from the hole edge at the surface and at the mid-thickness. [(a) At the surface and (b) At the mid-thickness]

+Figure 18 Relationship between the resultant force and the applied vertical displacement.

Figure 19 Distribution of equivalent plastic strain when the applied displacement is 0.5 mm.

Figure 20 Examples of the integral domains for the problem of cold working followed by the tensile deformation. The radius ε of the inner region Ω_ε^o is 0.5 mm. [(a) r^o = 1.9 mm, (b) r^o = 3.8 mm, and (c) r^o = 5.7 mm]

Figure 21 Variations of the evaluated J-integral values along the crack front for the problem of the cold work followed by the tensile deformation. [(a) Applied displacement: 0.20 mm, and (b) Applied displacement: 0.50 mm]

Figure 22 Geometry of the CT specimen and its simplified model. [(a) Geometries and the dimensions of the CT specimen, and (b) Simplified model of the CT specimen]

Figure 23 Finite element discretization of the simplified CT specimen. [(a) Overall view of the FE model, (b) Magnified view of the vicinity of the crack, and (c) Crack face]

Figure 24 Variations of the Young's modulus and the yield stress.

Figure 25 Outer surfaces of small, medium, and large integral domains with ε = 1.0 mm. [(a) Small, (b) Medium, and (c) Large]

Figure 26 Load-displacement relationship for the case of homogeneous material.

Figure 27 Deformation and distributions of equivalent plastic strain at a displacement of 3.0 mm. [(a) Overall side view, and (b) Magnified view of the vicinity of the crack front]

Figure 28 Distributions of the evaluated J-integral values along the crack front for various radii ε of near the crack from domain Ω_ε^o and for two magnitudes of the deformations of the CT specimen (0.03 mm and 3.0 mm). [(a) Displacement 0.03 mm and $\varepsilon = 0.5$ mm, (b) Displacement 3.0 mm and $\varepsilon = 0.5$ mm, (c) Displacement 0.03 mm and $\varepsilon = 1.0$ mm, and (f) Displacement 3.0 mm and $\varepsilon = 1.0$ mm]

Figure 29 Load-displacement curves. [(a) Decreasing yield stress and Young's modulus and (b) Increasing yield stress and Young's modulus]

Figure 30 Deformations and the distributions of the equivalent plastic strain for the cases

of decreasing and increasing yield stress and Young's modulus in the vicinity of the crack front. [(a) Case of decreasing yield stress and Young's modulus in the vicinity of the crack front (left: overall view, and right: vicinity of the crack front), and (b) Case of increasing yield stress and Young's modulus in the vicinity of the crack front (left: overall view, and right: vicinity of the crack front)]

Figure 31 Distributions of the evaluated J-integral values along the crack front. [(a) Decreasing yield stress and Young's modulus; load line displacement: 0.03 mm, (b) Increasing yield stress and Young's modulus; load line displacement: 0.03 mm, (c) Decreasing yield stress and Young's modulus; load line displacement: 3.00 mm, and (d) Increasing yield stress and Young's modulus; load line displacement: 3.00 mm]